ABSTRACT

Title of thesis: ENERGY CONVERSION IN NANOCHANNELS GRAFTED WITH POLYELECTROLYTE AND POLYZWITTERION BRUSHES

Jahin Patwary

Thesis directed by: Dr. Siddhartha Das
Department of Mechanical Engineering

A continuous mission in the sciences is the never-ending search for more energy and fuel. As time brings the reality of how limited natural resources are, we seek to expand to more synthetic methods of preserving and converting energy. Prevalent applications of renewable energy include solar energy, wind power, tidal power, and hydropower to list a few. It is no surprise that several of these applications stem from the involvement of fluid flow and the fluid pressure. This thesis explores a specific method of energy conversion in charged nanochannel flows of electrolytic solution, a subject that has gained great attention in recent years.

This particular method of nanofluidic energy conversion inside a charged nanochannel is an example of *Electrokinetic Energy generation* in pressure-driven liquid trans-

port. A charged nanochannel in contact with an electrolyte solution develops an *Electric Double Layer (EDL)* of charge where the number of counterions (ions of charge opposite in sign to that of the nanochannel wall) is much larger than the number of coions (ions of charge identical in sign to that of the nanochannel wall) in order to screen the wall charge. In presence of a pressure-driven flow, the ions within the EDL are advected downstream. The counterions number density being much larger than the coions, such a downstream migration would imply the accumulation of a net charge in the downstream direction, thereby triggering an axial electric field. This electric field when multiplied with the current generated due to the streaming of the ions would lead to an energy generation – this energy generation is effectively an example of *Electrochemomechanical Energy conversion*, where the mechanical energy of the pressure-driven flow and the chemical energy of the EDL gets converted into an electrical energy.

The purpose of this thesis is to explore the such *Electrokinetic Energy Conversion* in nanochannels grafted with pH-responsive charged polyelectrolyte (PE) brushes.

Grafting of nanochannels with polyelectrolyte (PE) brushes, invariably attribute a "smartness" to the nanochannels that have been used for a plethorsa of applications ranging for ion and biosensing, gating of ion transport, current rectification, fabrication of nanofluidic diodes and nano-actuators, etc. All these applications strictly depend on the modification of the *ionic current* by the presence of the PE brushes. On the contrary, the energy generation/conversion that we study here is a rare example where we utilize the *Electrohydrodynamic* (EHD) transport in brush-functionalized

nanochannels.

In this thesis, we experiment with parameters that would provide significant electrochemomechanical energy conversion in the presence of a pressure-driven background transport. We've gathered the optimal parameters to result in a 4-5% energy conversion efficiency. This is possible when the PE brushes exhibit a pH-dependent charge density.

Further, we extend our research by determining the possible electrochemomechanical energy conversion in a nanochannel grafted with polyzwitterionic (PZI) brushes. PZI brushes are capable of inducing a significantly high charge on both acidic and basic solutions.This allows electrokinetic induced power to be accessible over a wide range of pH values, as opposed to being confined to a narrow pH range compared to other EDL channels.

This thesis therefore sheds light on the smartness of nanochannels and their capabilities to generate power. We anticipate that our results will be able to provide a way for energy to be induced and produced in nanochannel-related applications, and maybe even find means to be a measure for developing more sustainable energy in larger scale applications.

ENERGY CONVERSION IN NANOCHANNELS GRAFTED WITH POLYELECTROLYTE AND POLYZWITTERION BRUSHES

by

Jahin Patwary

Thesis submitted to the Faculty of the Graduate School of the
University of Maryland, College Park in partial fulfillment
of the requirements for the degree of
Master of Science
2018

Advisory Committee:
Associate Professor Amir Riaz
Assistant Professor Taylor Woehl
Assistant Professor Siddhartha Das, Chair/Advisor

© Copyright by
Jahin Patwary
2018

Acknowledgments

I would like to acknowledge my advisor, Dr. Siddhartha Das, for not only taking me into his lab, but for always pushing me and never giving up on me. Even during times when things seemed difficult, Dr. Das found a way to make it seem much easier. I've felt more like a family member and a friend more so than just a student in Dr. Das' lab. My work would not have been possible without the help of all my lab mates: Shayandev Sinha, Harnoor Singh, Haoyuan Jing, Parth Desai, Yanbin Wang, and Kunal Ahuja. I would like to give a big shoutout to Guang Chen who has guided me and helped me so much with my graduate research. It is thanks to the countless hours I've spent working with Guang that I've been able to reach my goal today. I would like to thank the LSAMP Bridge to Doctorate Fellowship for funding my graduate studies and providing me the gateway to transition into graduate school with the knowledge, friends, and support I needed. Finally, I'd like to thank my parents, family, and friends for always pushing me and keeping me motivated throughout my pursuits in life.

Table of Contents

List of Figures

Chapter 1: Introduction

This chapter serves as a gateway about polymer chains and their relation to polyelectrolyte (PE) brushes. We briefly discuss the interactions that the polymer/polyelectrolyte chains exhibit to attain the brush-like configuration. This is followed by detailing the interaction of a PE brush with the electric double layer (EDL) within a nanochannel, which in turn serves as a key interaction to various applications in nanochannels grafted with the PE brushes. We further elaborate a certain kind of application of PE-grafted brushes in nanochannels: electrochemomechanical energy conversion in the presence of a pressure-driven flow. Finally, we address the main agenda and the organization of this.

1.1 Basics and applications of Polymer and Polyelectrolyte Brushes

Polymer chains exhibit unique behaviors dependent on their surrounding environment. When engulfed in a "good" solvent, these chains are attracted to the environment rather than each other. The repulsion of polymers from each other forces them to attain coil-like configuration in bulk solution [1]. Things change when the same polymer chains are grafted on a solid-liquid interface so close to one another that they cannot adopt their coil-like configuration without touching each other. Un-

der such circumstances, excluded volume effect sets in and enforces an avoidance of the adjacent polymer molecules by making it stretch in a direction perpendicular to the grafting surface and hence adopting a "brush"-like configuration [2–12]. Under such circumstances the brush configuration can be obtained by balancing the elastic and excluded volume energies. For the PE brushes, there is also the electrostatic repulsion energy between the polymer segments and the energy associated with the induced EDL. The overall configuration is dictated by a balance of these effects.

Understanding the free energy of a polyelectrolyte brush gives us the ability to decouple its elastic and excluded volume effects from the electrostatic effects [13–20]. Decoupling ensures that the brush height is independent of electrostatic effects. This allows us to focus on the electrostatic effects induced from the interaction of the polyelectrolyte brush with an electric double layer (EDL). The electrostatics from an EDL charges a PE brush and allows the brush to respond differently based on the surrounding pH, pKa, pKb, salt concentration, monomer distribution, and so on. By fine-tuning these parameters in an EDL, polyelectrolyte brushes can be used for different applications, including flow-valving action, flow control, drug delivery system, ion sensing and manipulation, biosensing, current rectification, fabrication of nanofluidic diodes, and several others (provide references for each applications; follow some of my papers).

1.2 Energy conversion in nanochannels grafted with polyelectrolyte brushes

It is clear that the PE brush grafting can render incredible "smartness to nanochannels. The nature of the grafted PE brushes and alteration of their configuration as a response to system parameters renders incredible flexibility in their application. While such widespread application of PE-brush-grafted nanochannels involving ion transport is known, relatively less is known about applications involving fluid transport. Recently, PE-grafted nanochannels have been shown to be an excellent electrochemomechanical energy converter [1, 13]-such conversion refers to the generation of an electrical energy caused by the triggering of the streaming electric field (or streaming potential) in the presence of a background nanofluidic pressure-driven transport [21, 22] migrating the charge density of the induced electric double layer (or EDL). It is worthwhile to note that while there have been many studies on streaming potential calculations in PE-grafted channels [23–32], we highlighted the manner in which such streaming potential generation will lead to highly efficient energy conversion in nanochannels with PE grafting. Our approach takes the free energy of the PEL, and then we decouple the electrostatic effects from the excluded volume and entropic effects in the nanochannel to quantify the energy conversion efficiency in polyelectrolyte brushes. Such a step is essential to describe the electrokinetics of the PE-brush-grafted nanochannels assuming a constant PE brush height that is independent of the pH and the salt concentration. Finally, we extend this analysis

in nanochannels grafted with polyzwitterionic brushes to ensure an enhanced energy generating capability of the nanochannels over a larger range of the pH values.

1.3 Main agenda of the present thesis

Our work focuses on establishing that such "soft" nanochannels can be employed for highly efficient, streaming-current-induced electrochemomechanical energy conversion in the presence of a background pressure-driven transport. In this thesis, we first decouple the electrostatic effects from the excluded volume and entropic effects in the free energy of a nanoconfined PE brush layer. We extend our calculation for the practically realizable situation when the PE brush layer, grafted on the inner walls of the nanochannel, demonstrates a pH-dependent charge density. Consideration of such pH dependence necessitates consideration of hydrogen and hydroxyl ions in the electric double layer charge distribution, cubic distribution of the monomer profile, and a PE layer-induced drag force that accounts for this given distribution of the monomer profile. Subsequently, we extend our analysis to polyzwitterion-grafted nanochannels. Our results express a hitherto unknown dependence of the streaming electric field (or the streaming potential) and the efficiency of the resultant energy conversion on parameters such as the pH of the surrounding electrolyte and the pKa and the pKb of the ionizable group that ionizes to produce the PE charge—we demonstrate using an integro-differential equation that the energy conversion efficiency substantially increases with an increase in the pH and the PE layer thickness. Similarly, this energy conversion is also concurrent during a decrease in the pKa and ion concentration of

the nanochannel fluid. We anticipate that our calculations will provide the design basis for a new form of nanochannel based electrical energy generator by utilizing the mechanical energy of the fluid flow and the chemical energy of the electric double layer.

1.4 Organization of the thesis

Chapter 2 focuses of energy conversion in nanochannels grafted with polyelectrolyte brushes. First we bridge the relation between this research and previous studies. We go into detail about the layout of a nanochannel grafted with PE brushes, including the ions in the electrolyte solution as well as the drag produced inside the channel. This helps break down the difference free energies of the system coming from the free energy of the PE brush and the free energy of the EDL. By using a decoupling method, the free energy of the electrostatics can be separated from the excluded volume and entropic effects, giving way to simplify the derivations for the governing equations of electrostatic potential in the system. We then focus on the calculation of the velocity field by assuming a steady, uni-directional, and hydrodynamically fully developed flow. This provides us with the dimensionless governing equations and the boundary conditions of the velocity field, but the calculation of the streaming electric field is required to solve this equation. We obtain the net ionic current first and then solve for the streaming electric field. We use the method of solving an integro-differential equation to solve for both the streaming potential and the velocity field. Lastly, we solve for the energy conversion efficiency and provide

the corresponding plots to demonstrate how much electrochemomechanical energy is converted. Chapter 3 demonstrates a very similar method to solve for this conversion efficiency, but as we are dealing with polyzwitterionic (PZI) brushes, we must account for both the negative and positive charges on the brushes. This reactivity requires us to address the charge interactions and resulting streaming potential, velocity field, and streaming electric field in both acidic and basic solutions. After providing the resulting plots, both chapters further discuss applications of the findings, and dive into possible future works.

Chapter 2: Efficient electrochemomechanical energy conversion in nanochannels grafted with polyelectrolyte layers with pH-dependent charge density

Nanochannels, functionalized by grafting with a layer of charged polyelectrolyte (PE), have been employed for a large number of applications such as flow control, ion sensing, ion manipulation, current rectification, nanoionic diode fabrication, and many more. Recently, we established that such PE-grafted nanochannels, often denoted as a "soft" nanochannels, can be employed for highly efficient, streaming-current-induced electrochemomechanical energy conversion in presence of a background pressure-driven transport. In this chapter,[1] *we extend our calculation for the practically realizable situation when the PE layer demonstrates a pH-dependent charge density. Consideration of such pH-dependence necessitates consideration of hydrogen and hydroxyl ions in the electric double layer charge distribution, cubic distribution of the monomer profile, and a PE-layer-induced drag force that accounts for this given distribution of the monomer profile. Our results express a hitherto unknown depen-*

[1]Contents of this chapter have been published as: *J. Patwary, G. Chen and S. Das, Efficient electrochemomechanical energy conversion in nanochannels grafted with polyelectrolyte layers with pH?dependent charge density. Microfluid. Nanofluid., Vol. 20, pp. 37 (2016).*

dence of the streaming electric field (or the streaming potential) and the efficiency of the resultant energy conversion on parameters such as the pH of the surrounding electrolyte and the pK_a of the ionizable group that ionizes to produce the PE charge – we demonstrate that increase in the pH and the PE layer thickness and decrease in the pK_a and the ion concentration substantially enhance the energy conversion efficiency.

2.1 Introduction

Our previous study considered a most simplified situation where the PE molecules were assumed to have a constant charge density and the drag coefficient was assumed to be independent of the monomer distribution [13, 19]. In the proposed study, we provide a much more realistic treatment of this problem by assuming that the PE molecule exhibits pH-dependent charge density. Such a consideration leads to three distinct issues. Firstly, we need to account for the hydrogen and hydroxyl ion distribution in the electric double layer (EDL) ionic distribution, with the EDLs forming on both sides of the PE layer-electrolyte interface. Secondly, such pH dependence necessitates consideration of a cubic monomeric distribution of the grafted PE molecule in order to address the unphysical discontinuities in the hydrogen ion concentration profile associated with the consideration of uniform monomer distribution [1, 16, 18, 33]. Finally, this cubic monomeric profile is considered while expressing the monomer distribution dependence of the drag coefficient for the fluid flow [18, 33]. Our theoretical framework is based on first calculating the electrostatics of the PE-electrolyte interface, with the PE being grafted as "brushes" [5, 6, 10] on the inner walls of the

nanochannel. We assume that the PE electrostatic contribution is decoupled from the elastic and the excluded volume contributions of the PE molecule. This allows us to assume a constant thickness of the PE layer (i.e. the thickness is decided solely by the balance of the elastic and excluded volume effects) while calculating the EDL electrostatics of the PE-electrolyte interface. In a couple of recent studies, we have quantitively established the physical conditions (or parameter space) that allow such decoupling for the PE layers grafted on the inner walls of a nanochannel and forming "brushes" that have a height smaller than the nanochannel half height [1,33]. Therefore, in the present study we work in this parameter space. This EDL electrostatics is subsequently used to calculate the velocity field, streaming potential, and the efficiency of the energy conversion. The salient issue here is that we obtain the velocity field by solving an integro-differential equation, which stems from the fact that the streaming electric field is not explicitly expressible in terms of the pressure-driven and electroosmotic (due to the streaming electric field) transport. We have used such integro-differential approach in one of our previous papers [19]; here, we provide a more rigorous analysis that accounts for the contribution of H^+ and OH^- ions and at the same time account for the monomer distribution-dependent drag force [18,33–35]. Our analyses express the hitherto unknown dependences of the streaming current and the efficiency in a PE-grafted nanochannel on factors such as the pH and the pKa (of the acid that dissociates to produce the negative charge of the PE layer). Our results further demonstrate a significantly high (4-5%) efficiency of the electrochemomechanical energy conversion [36,37] associated with the generation of the streaming electric field in PE-grafted nanochannels with pH-dependent charge density. This efficiency

number is reasonable in the light of the experimental result on the streaming-electric-field-induced electrochemomechanical energy conversion (predicting an efficiency of approximately 3%. [36]) and establishes the nanochannel with grafted PE layer with pH-dependent charge density as an important device for nanofluidic electrochemomechanical energy conversion.

2.2 Theory

We consider a pressure-driven transport of an electrolyte solution in a soft charged nanochannel of height $2h$ (see Figure 2.1) and study the streaming electric field and the efficiency of the resulting electrochemomechanical energy conversion. This "softness" of the nanochannel is attributed to a layer of wall-grafted ion-penetrable charged polyelectrolyte (PE) layer of thickness d (see Figure 2.1). The grafting density is assumed to be large enough to ensure that the grafted PE molecules attain a brush-like configuration. [5,6,38] The charge on the PE layer is attributed to the pH-dependent ionization of the PE molecules; this ensures that the charge density of the PE layer is pH-dependent. This charging triggers an EDL ion distribution at either sides of the PE-layer-electrolyte interface. We shall first briefly discuss the EDL electrostatics of the system, which has already been discussed in details in our previous papers; [1,16,18] this will be followed by the calculations of the velocity field, the streaming electric field, and the energy conversion efficiency.

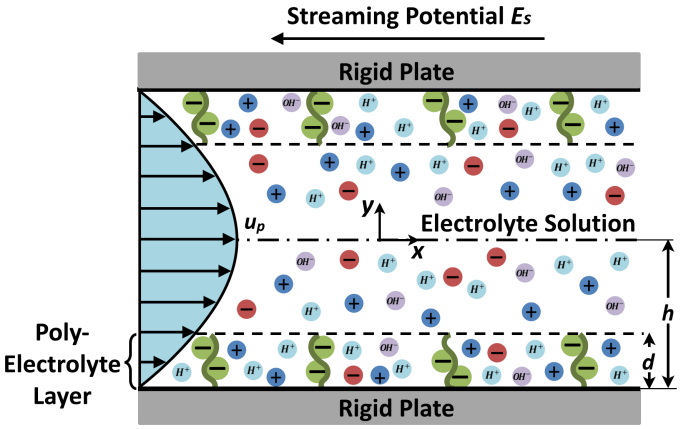

Figure 2.1: *Schematic of the pressure-driven transport in a nanochannel grafted with negatively charged pH-sensitive PE layer. In this schematic, we also show the direction of the streaming electric field or streaming potential* E_S.

2.2.1 Electrostatics

The total free energy change (ΔF) associated with a grafted PE molecule system forming an EDL can be expressed as:

$$\Delta F = \Delta F_{PE} + \Delta F_{EDL}, \tag{2.1}$$

where ΔF_{PE} is the free energy change associated with a single grafted PE molecule and ΔF_{EDL} is the free energy change associated with the EDL formation. One can express ΔF_{PE} as:

$$\Delta F_{PE} = \Delta F_{PE,ent} + \Delta F_{PE,EV} + \Delta F_{PE,elec}, \tag{2.2}$$

where $\Delta F_{PE,ent}$, $\Delta F_{PE,EV}$, and $\Delta F_{PE,elec}$ are the free energy changes associated with the entropic (or elastic), excluded volume, and electrostatic contributions of the PE molecule. Calculations considering eq.(2.1) and eq.(2.2) simultaneously have been

provided before; [39, 40] however, these calculations may be inappropriate for cases where the PE charge density is a function of the pH. [16,18,41] This inappropriateness stems from enforcing the H^+ ion concentration to obey the Boltzmann distribution both inside and outside the PE layer; such a consideration is incorrect and leads to unphysical discontinuities in the value and in the gradient of the H^+ ion concentration at the PE-layer-electrolyte interface, as established by our previous study. [16] The correct formulation that considers both eqs.(2.1,2.2) and at the same time provides a physically consistent description of the H^+ ion concentration is still unknown. In several recent papers, we have proposed a simplified formulation where we have described the PE-layer EDL electrostatics in a framework that decouples the PE elastic and excluded volume effects from the PE electrostatic effects. [13–20] Such an assumption ensures that the PE layer height is dictated entirely by the balance of the elastic and the excluded volume effects, and is hence independent of the electrostatic and the EDL effects. Please note there have been a plethora of studies that have modelled the electrostatics and the electrokinetics of PE-grafted interfaces assuming a constant thickness of the PE layer (see the review papers [42–47] and the articles cited in these review papers). All these calculations, therefore, have implicitly assumed such decoupling of the PE electrostatic effects from the PE elastic and excluded volume effects. Only very recently, we provided the physical conditions and the parameter space corresponding to which such de-coupling is possible. [1, 33] We refrain from discussing this parameter space in details here; however, we do assume that the present study is described in the same parameter space making the decoupling feasible.

Under these conditions, the free energy change associated with PE electrostatic

effect and that associated with the resulting EDL formation must individually balance each other. Therefore, one may write:

$$\Delta F' = \Delta F_{PE,elec} + \Delta F_{EDL}. \tag{2.3}$$

Please note that $\Delta F' \approx \Delta F$ for $\Delta F_{PE,elec} \gg \left(\Delta F_{PE,ent} + \Delta F_{PE,EV}\right)$, whereas $\Delta F' \ll \Delta F$ for $\Delta F_{PE,elec} \ll \left(\Delta F_{PE,ent} + \Delta F_{PE,EV}\right)$. In our previous studies we have derived the equilibrium EDL electrostatics starting from eq.(2.3). [1,16] Here we briefly summarize these steps for the sake of completeness. Eq.(2.3) can be re-written as:

$$\Delta F' = \int \Delta f \left(\psi, \psi', n_{\pm}, n_{H^+}, n_{OH^-}\right) d^3\mathbf{r}, \tag{2.4}$$

where Δf is the density of the free energy change, expressed as (considering the bottom half of the nanochannel):

$$\Delta f = k_B T \sum_i \left[n_i \left(\ln\left(\frac{n_i}{n_{i,\infty}}\right) - 1 \right) \right] - \frac{\epsilon_0 \epsilon_r}{2} |\nabla\psi|^2 + e\psi \left[\sum_i z_i n_i - \varphi n_{A^-} \right]$$

$$(-h \le y \le -h + d),$$

$$\Delta f = k_B T \sum_i \left[n_i \left(\ln\left(\frac{n_i}{n_{i,\infty}}\right) - 1 \right) \right] - \frac{\epsilon_0 \epsilon_r}{2} |\nabla\psi|^2 + e\psi \left[\sum_i z_i n_i \right] \quad (-h + d \le y \le 0). \tag{2.5}$$

In eq.(2.5) in the right hand side, the first term represents the entropic contribution due to the mixing of of the ions, the second term represents the self energy of the EDL electric field, and the third term represents the electrostatic energy of the PE ions (valid only within the PE layer) electrolyte, hydrogen, and hydroxyl ions. Further ψ is the electrostatic potential, ϵ_0 is the permittivity of free space, ϵ_r is the relative permittivity of the medium, $k_B T$ is the thermal energy, e is the electronic charge, z_i,

n_i and $n_{i,\infty}$ are the valence, the number density and the bulk number density of ion of type i ($i = \pm, H^+, OH^-$). Here the electrolyte salt is assumed to be monovalent and symmetric (hence $z_+ = -z_- = 1$). Also in eq.(2.5), n_{A^-} is the number density of the negatively charged PE ions. Further, $\varphi(y)$ is the dimensionless monomer distribution, which should obey a *non-unique* cubic distribution in y (detailed later) in order to avoid unphysical discontinuities associated with considering a constant φ for a PE layer with pH-dependent charge density [16, 18]. The number densities of the negatively charged PE ions depend on local H^+ ion concentration and can be expressed as:

$$n_{A^-} = \frac{K'_a \gamma_a}{K'_a + n_{H^+}}. \tag{2.6}$$

Here the anionic charge of the negatively charged PE layer is attributed to the ionization of the acid HA ($HA \leftrightarrow H^+ + A^-$; ionization constant K_a). Also in eq.(2.6), γ_a is the maximum site density of the chargeable groups of the PE layer and $K'_a = 10^3 N_A K_a$ (N_A is the Avogadro number). Please note that eq.(2.5) is based on the assumption that the EDL is described by the mean-field electrostatics. Therefore, issues such as ion-ion correlations have not been considered. In fact, effects such as the consideration of finite ion sizes and finite solvent polarizability – these effects can be modelled within the mean-field framework – have also been neglected.

Governing equations are obtained by minimizing eq.(2.4) with respect to the variables ψ, $n_\pm$, n_{H^+} and n_{OH^-}. This eventually allows us to write (see Chen and Das [1, 16] for detailed derivation) the equations governing the equilibrium as:

$$\bar{n}_{\pm} = \exp\left(\mp\bar{\psi}\right) \qquad [\text{for} -1 \le \bar{y} \le 0] \tag{2.7}$$

$$\bar{n}_{OH^-} = \left(\bar{n}_{OH^-,\infty}\right)\exp\left(\bar{\psi}\right) \qquad [\text{for} -1 \le \bar{y} \le 0] \tag{2.8}$$

$$\begin{aligned} \bar{\psi} &= -\frac{\ln\left(\frac{\bar{n}_{H^+}}{\bar{n}_{H^+,\infty}}\right)}{1+\frac{\bar{K}'_a\bar{\gamma}_a\varphi}{\left(\bar{K}'_a+\bar{n}^+_H\right)^2}} \qquad \left[\text{for} -1 \le \bar{y} \le -1+\bar{d}\right], \\ \bar{\psi} &= -\ln\left(\frac{\bar{n}_{H^+}}{\bar{n}_{H^+,\infty}}\right) \qquad \left[\text{for} -1+\bar{d} \le \bar{y} \le 0\right]. \end{aligned} \tag{2.9}$$

$$\begin{aligned} \frac{d^2\bar{\psi}}{d\bar{y}^2} &= \frac{1}{2\bar{\lambda}^2}[-\exp(-\bar{\psi}) + (1+\bar{n}_{H^+,\infty})\exp(\bar{\psi}) + (\bar{n}_{OH^-,\infty})\exp(\bar{\psi}) \\ &\qquad -\bar{n}_{H^+} + \frac{\bar{K}'_a\bar{\gamma}_a\varphi}{\bar{K}'_a+\bar{n}_{H^+}}] \qquad \left[\text{for} -1 \le \bar{y} \le -1+\bar{d}\right], \\ \frac{d^2\bar{\psi}}{d\bar{y}^2} &= \frac{1}{2\bar{\lambda}^2}[-\exp(-\bar{\psi}) + (1+\bar{n}_{H^+,\infty})\exp(\bar{\psi}) + (\bar{n}_{OH^-,\infty})\exp(\bar{\psi}) \\ &\qquad -\bar{n}_{H^+,\infty}\exp\left(-\bar{\psi}\right)] \qquad \left[\text{for} -1+\bar{d} \le \bar{y} \le 0\right]. \end{aligned} \tag{2.10}$$

In the above equations, $\bar{y} = \frac{y}{h}$, $\bar{d} = \frac{d}{h}$, $\bar{\psi} = \frac{e\psi}{k_BT}$, $\bar{n}_{\pm} = n_{\pm}/n_{\infty}$ (we assume $n_{+,\infty} = n_{-,\infty} = n_{\infty}$), $\bar{n}_{H^+} = \frac{n_{H^+}}{n_{\infty}}$, $\bar{n}_{OH^-} = \frac{n_{OH^-}}{n_{\infty}}$, $\bar{n}_{H^+,\infty} = \frac{n_{H^+,\infty}}{n_{\infty}}$, $\bar{n}_{OH^-,\infty} = \frac{n_{OH^-,\infty}}{n_{\infty}}$, $\bar{K}'_a = \frac{K'_a}{n_{\infty}}$, $\bar{\lambda} = \frac{\lambda}{h}$ (where $\lambda = \sqrt{\frac{\epsilon_0\epsilon_r k_BT}{2n_{\infty}e^2}}$ is the EDL thickness).

Eq. (2.10) uses the Boltzmann distribution [see eqs.(2.7,2.8,2.9)] to express the distribution of $\bar{n}_{\pm}$, $\bar{n}_{OH^-}$, and $\bar{n}_{H^+}$ (outside the PE layer). On the other hand, eq.(2.9) clearly shows that H^+ ion distribution, on account of its reaction that causes the PE charging, does not obey the Boltzmann distribution within the PE layer – this has been the most important identification of our analysis of the EDL electrostatics of PE-grafted interfaces. [1, 16, 18] The other important issue of eq.(2.10) is the manner

in which $n_{i,\infty}$s are defined. We assume addition of an acid that furnishes the same anion as the anion of the electrolyte salt. As a result, we may write: $n_{+,\infty} = n_\infty$ and $n_{-,\infty} = n_\infty + n_{H^+,\infty}$. Eqs. (2.9, 2.10) need to be solved simultaneously in presence of the following dimensionless boundary conditions:

$$\begin{aligned}
&\left(\frac{d\bar{\psi}}{d\bar{y}}\right)_{\bar{y}=-1} = 0; \qquad \left(\frac{d\bar{\psi}}{d\bar{y}}\right)_{\bar{y}=0} = 0 \\
&\left(\bar{\psi}\right)_{\bar{y}=(-1+\bar{d})^+} = \left(\bar{\psi}\right)_{\bar{y}=(-1+\bar{d})^-}; \\
&\left(\frac{d\bar{\psi}}{d\bar{y}}\right)_{\bar{y}=(-1+\bar{d})^+} = \left(\frac{d\bar{\psi}}{d\bar{y}}\right)_{\bar{y}=(-1+\bar{d})^-}.
\end{aligned} \tag{2.11}$$

Finally, the monomer density distribution $\varphi(y)$ is so selected that along with eq.(2.9) it ensures that eq.(2.11) leads to the following set of Boundary Conditions for $\bar{n}_{H^+}$:

$$\begin{aligned}
&\left(\frac{d\bar{n}_{H^+}}{d\bar{y}}\right)_{\bar{y}=-1} = 0; \qquad \left(\frac{d\bar{n}_{H^+}}{d\bar{y}}\right)_{\bar{y}=0} = 0 \\
&\left(\bar{n}_{H^+}\right)_{\bar{y}=(-1+\bar{d})^+} = \left(\bar{n}_{H^+}\right)_{\bar{y}=(-1+\bar{d})^-}; \\
&\left(\frac{d\bar{n}_{H^+}}{d\bar{y}}\right)_{\bar{y}=(-1+\bar{d})^+} = \left(\frac{d\bar{n}_{H^+}}{d\bar{y}}\right)_{\bar{y}=(-1+\bar{d})^-}.
\end{aligned} \tag{2.12}$$

Eq.(2.9) is used in eq.(2.10) to eliminate $\bar{\psi}$ and express the differential equation entirely in terms of $\bar{n}_{H^+}$; this equation is subsequently solved in presence of eq.(2.12) to obtain the distribution of $\bar{n}_{H^+}$. This distribution is next used in eq.(2.9) to obtain the corresponding distribution of $\bar{\psi}$. Finally, the monomer distribution φ, in addition to ensuring the attainment of eq.(2.12) from eq.(2.11), must also ensure [10, 39]

$$\frac{1}{\sigma a^3}\int_{-h}^{-h+d} \varphi(y)dy = N, \tag{2.13}$$

where σ is the grafting density (having units of $1/m^2$), a is the Kuhn length (hence the volume of a monomer segment is $\sim a^3$), and N is the size (or the number of

monomers) of a PE molecule. All these criteria are satisfied by a *non-unique* cubic distribution of φ expressed as (see Chen and Das [16] for detailed derivation):

$$\varphi(y) = \left(\frac{Na^3\sigma}{d}\right)\left(\frac{4}{\bar{d}^3}\right)\left(\bar{y}+1-\bar{d}\right)^2\left(\bar{y}+1+\frac{\bar{d}}{2}\right). \tag{2.14}$$

2.2.2 Calculation of the Velocity Field

We consider a pressure-driven background transport in this PE-grafted nanochannel. The flow is assumed to be steady, uni-directional and hydrodynamically fully-developed. Such nanochannel pressure-driven transport leads to a downstream migration of the mobile ions of the EDL, which in turn gives rise to the well-known streaming electric field or streaming potential E_S. [48–51] This electric field is in a direction opposite to the pressure-driven transport and gives rise to an induced electroosmotic transport that opposes the pressure-driven transport. Under these conditions, the velocity field u can be expressed as:

$$\begin{aligned}
&\eta\frac{d^2u}{dy^2} - \frac{dp}{dx} + e(n_+ - n_- + n_{H^+} - n_{OH^-})E_S - \mu_c u = 0 \\
&\qquad\qquad [-h \le y \le -h+d]\,, \\
&\eta\frac{d^2u}{dy^2} - \frac{dp}{dx} + e(n_+ - n_- + n_{H^+} - n_{OH^-})E_S = 0 \\
&\qquad\qquad [-h+d \le y \le 0]\,.
\end{aligned} \tag{2.15}$$

In eq.(3.19), dp/dx is the employed pressure gradient, η is the dynamic viscosity of the liquid, and $\mu_c = (\frac{\varphi(y)}{b})^2$ (b is a parameter that has a unit of $length/\sqrt{viscosity}$) is the drag coefficient within the PE layer. Eq. (3.19) is expressed under several simplifying assumptions. Firstly, we assume that the background flow field does not

alter the shape of the grafted PE layer under steady state. Secondly, the timescale (τ_{EDL}) of distribution of the EDL ions ($\tau_{EDL} \sim \lambda^2/D_{ion} \sim\ 10^{-10} - 10^{-6}\ s$, with EDL thickness $\lambda \sim 1 - 100\ nm$ and ion diffusivity $D_{ion} \sim 10^{-8}\ m^2/(Vs)$) is considered much smaller than the time scale associated with the pressure-driven liquid transport. This assumption allows us to consider the EDL ion distribution as quasi-steady with respect to the flow field, thereby sufficing to express the flow field through eq.(3.19) without requiring the coupled Poisson-Nernst-Planck and Navier-Stokes equations to describe the flow field and ion transport. [41] Finally, in eq.(3.19) the drag coefficient (μ_c) is expressed assuming that $\mu_c \sim K^2$, where K^{-1} (which varies as φ^{-1}) is the length that screens the background flow from the flow inside the grafted PE molecules. This analysis is borrowed from the idea of flow screening between the inside and the outside of a polymer coil where the background flow velocity is much larger than the velocity inside the polymer coil; [52–54] the justification of applying this analysis to the present case of grafted PE molecules is that the PE molecules (just like the polymer coil), being grafted, will have a velocity that is much smaller than the background velocity.

Eq.(3.19) can be expressed in dimensionless form as:

$$\begin{aligned}
&\frac{d^2\bar{u}}{d\bar{y}^2} + \frac{u_r}{2\bar{\lambda}^2}\bar{E}_S[\exp(-\bar{\psi}) - (1+\bar{n}_{H^+,\infty})\exp(\bar{\psi}) - \bar{n}_{OH^-,\infty}\exp(\bar{\psi}) \\
&\qquad +\bar{n}_{H^+}] - \bar{\alpha}^2\varphi^2\bar{u} = 1 \qquad \left[-1 \le \bar{y} \le -1+\bar{d}\right], \\
&\frac{d^2\bar{u}}{d\bar{y}^2} + \frac{u_r}{2\bar{\lambda}^2}\bar{E}_S[\exp(-\bar{\psi}) - (1+\bar{n}_{H^+,\infty})\exp(\bar{\psi}) - \bar{n}_{OH^-,\infty}\exp(\bar{\psi}) \\
&\qquad +\bar{n}_{H^+,\infty}\exp(-\bar{\psi})] = 1 \qquad \left[-1+\bar{d} \le \bar{y} \le 0\right].
\end{aligned} \tag{2.16}$$

In eq. (2.16), $\bar{u} = \frac{u}{u_{p,0}}$ (where $u_{p,0} = \frac{h^2}{\eta}\frac{dp}{dx}$ is pressure-driven velocity scale), $u_r = \frac{u_{e,0}}{u_{p,0}}$ (where $u_{e,0} = \frac{k_B T}{ez}\frac{\epsilon_0 \epsilon_r E_0}{\eta}$ is the electroosmotic velocity scale; E_0 is the scale of the electric field), $\bar{E}_S = \frac{E_S}{E_0}$, and $\bar{\alpha} = \frac{h}{b\sqrt{\eta}}$. Please note that eq.(2.16) uses the eqs.(2.7,2.8,2.9) to express the ion distributions. Solution of eq.(2.16) is sought in presence of the following dimensionless boundary conditions:

$$\begin{gathered}\left(\frac{d\bar{u}}{d\bar{y}}\right)_{\bar{y}=-1} = 0; \qquad \left(\frac{d\bar{u}}{d\bar{y}}\right)_{\bar{y}=0} = 0; \\ (\bar{u})_{\bar{y}=(-1+\bar{d})^+} = (\bar{u})_{\bar{y}=(-1+\bar{d})^-}; \\ \left(\frac{d\bar{u}}{d\bar{y}}\right)_{\bar{y}=(-1+\bar{d})^+} = \left(\frac{d\bar{u}}{d\bar{y}}\right)_{\bar{y}=(-1+\bar{d})^-}.\end{gathered} \tag{2.17}$$

Of course, the solution of $\bar{u}$ requires the value of the $\bar{E}_S$. Calculation of $\bar{E}_S$ is discussed in the following subsection.

2.2.3 Calculation of the Streaming electric field E_S

To obtain E_S, we consider that the net ionic current (per unit width) i is equal to zero, i.e.,

$$i = 2e\int_{-h}^{0} (u_+ n_+ - u_- n_- + u_{H^+} n_{H^+} - u_{OH^-} n_{OH^-})\, dy = 0, \tag{2.18}$$

where u_i $(i = \pm, H^+, OH^-)$ is the ion migration velocity, expressed as:

$$u_i = u + \frac{e z_i E_S}{f_i}. \tag{2.19}$$

Here f_i is the ionic friction coefficient for ion i. Using eqs.(2.7,2.8,2.9,2.19) in eq.(2.18), we finally obtain the dimensionless streaming electric field as:

$$\bar{E}_S = \frac{\int_{-1}^{0} \bar{u}\left[-\exp(-\bar{\psi}) + (1+\bar{n}_{H^+,\infty})\exp(\bar{\psi}) - \bar{n}_{H^+} + (\bar{n}_{OH^-,\infty})\exp(\bar{\psi})\right] d\bar{y}}{u_r \int_{-1}^{0}[R_+ \exp(-\bar{\psi}) + R_-(1+\bar{n}_{H^+,\infty})\exp(\bar{\psi}) + R_{H^+}\bar{n}_{H^+} + R_{OH^-}(\bar{n}_{OH^-,\infty})\exp(\bar{\psi})]d\bar{y}}, \tag{2.20}$$

where $R_i = \frac{e^2 z_i^2 \eta}{\epsilon_0 \epsilon_r k_B T f_i}$ is a dimensionless parameter, often interpreted as the inverse of the ionic Peclet number [48]. Please note that for the case where the electrolyte ion number density (n_∞) is much larger than the number density of H^+ and OH^- ions (i.e., $\bar{n}_{H^+} = \frac{n_{H^+}}{n_\infty} \ll 1$, $\bar{n}_{H^+,\infty} = \frac{n_{H^+,\infty}}{n_\infty} \ll 1$, and $\bar{n}_{OH^-,\infty} = \frac{n_{OH^-,\infty}}{n_\infty}$), eq.(2.20) reduces to:

$$\bar{E}_S = \frac{2}{u_r} \frac{\int_{-1}^{0} \bar{u} \sinh(\bar{\psi}) d\bar{y}}{R_+ \int_{-1}^{0} \exp(-\bar{\psi}) d\bar{y} + R_- \int_{-1}^{0} \exp(\bar{\psi}) d\bar{y}}. \tag{2.21}$$

We have obtained this exact same form of the streaming potential in our previous paper, [19] where we did not consider the effect of the H^+ and OH^- ions.

Since we do not have an explicit expression for $\bar{u}$, eq.(2.20) will imply that in order to obtain the velocity field $\bar{u}$ by using eq.(2.16), one needs to solve an integro-differential equation in $\bar{u}$. In other words, since $\bar{E}_S$ appearing in eq.(2.16) is expressed by using eq.(2.20), the result is an integro-differential equation in $\bar{u}$. Calculation of the streaming electric field by solving such an integro-differential equation was first performed by us in one of our recent studies; [19] in that study, [19] we computed the streaming electric field in a PE-grafted nanochannel with large constant charge densities (large enough to invalidate the use of Debye-Hückel linearization). In the present study, we address a much more complete problem, where this charge density is assumed to be pH-dependent, which in turn necessitates consideration of H^+ and OH^- ions

in the EDL ion distribution and enforces a particular distribution of the chargeable monomers of the PE molecule. It is worthwhile to note here that solution of such integro-differential equation is necessitated by the fact that it is not possible to express $\bar{u}$ as an explicit combination of the pressure-gradient and the electrostatic potential distribution $\bar{\psi}$; while such explicit formulation is standard for nanochannels without the PE grafting, [48–51] for nanochannels with PE grafting it is possible only for the special case of PE with constant pH-independent small charge densities (which allows the use of Debye-Hückel linearization). [13] This integro-differential equation is solved numerically in presence of the boundary conditions expressed in eq.(3.22). This numerical treatment requires application of a suitable iteration procedure; the starting guess profile of the iteration is typically the $\bar{u}$ profile obtained for the analytical case in our previous study. [13] Once $\bar{u}$ has been obtained by solving this integro-differential equation, we can use eq.(2.20) to obtain $\bar{E}_S$, given the fact that we already know the distribution of $\bar{\psi}$ and $\bar{n}_{H^+}$.

2.2.4 Calculation of efficiency of the electrochemomechanical energy conversion

Generation of the nanofluidic streaming current (i_S) and the streaming electric field (E_S) is a process of nanoscale electrochemomechanical energy conversion, [36,37] since the mechanical energy of the pressure-driven flow and the chemical energy of the EDL are converted to the electrical energy associated with the generation of i_S

and E_S. This efficiency ξ of this energy conversion can be expressed as:

$$\xi = \frac{P_{out}}{P_{in}}. \tag{2.22}$$

Here P_{in} and P_{out} are the input and the output powers (per unit area), expressed as:

$$\begin{aligned} P_{out} &= \frac{1}{4} i_S E_S, \\ P_{in} &= \left| -\frac{dp}{dx} \right| Q_{in}. \end{aligned} \tag{2.23}$$

Here

$$i_S = 2e \int_{-h}^{0} u \left(n_+ - n_- + n_{H^+} - n_{OH^-} \right) dy, \tag{2.24}$$

and Q_{in} is the the input volume flow rate per unit width, expressed as:

$$Q_{in} = 2 \int_{-h}^{0} u_p dy, \tag{2.25}$$

Here u_p is the pure pressure-driven velocity field expressed as $u_p = -\frac{dp}{dx}\frac{h^2}{2\eta}\left(1 - \frac{y^2}{h^2}\right)$. Using eqs.(2.7,2.8,2.9,3.28,3.29,3.31) in eq.(3.27), we can finally express ξ as:

$$\begin{aligned} &\xi = u_r \times \\ &\frac{\int_{-1}^{0} \bar{u} \left[\exp(-\bar{\psi}) - (1 + \bar{n}_{H^+,\infty}) \exp(\bar{\psi}) + \bar{n}_{H^+} - (\bar{n}_{OH^-,\infty}) \exp(\bar{\psi}) \right] d\bar{y}}{8\bar{\lambda}^2 \int_{-1}^{0} \bar{u}_p d\bar{y}} \end{aligned} \tag{2.26}$$

where $\bar{u}_p = u_p / u_{p,0}$. It is worthwhile to note here that this efficiency is calculated based on the actual input flow rate. There are examples, where the efficiency has been calculated based on the reduced flow rate, caused by the generation of the streaming-electric-field-induced electroosmotic transport that opposes the pressure-driven transport. [55, 56] Such a consideration leads to an *artificial* increase of the

efficiency, which is incorrect. Rather, this efficiency should always be calculated based on the input power and the input velocity as has been done by Daiguji et al. [36] as well as our previous study. [13]

2.3 Results

Figure 2.2 demonstrates the pH and the pK_a dependences of the dimensionless streaming electric field ($\bar{E}_S$) and the energy conversion efficiency ξ. Prior to discussing these dependences, we first discuss the corresponding dependence of the transverse variation of the dimensionless electrostatic potential ($\bar{\psi}$) on these parameters. We have provided this result on electrostatic potential in our previous studies; [1, 16] we repeat it here in order to better explain the nature of variation of $\bar{E}_S$ and ξ. Enhancement of the bulk pH (or pH_∞), which implies a decrease in the concentration of the H^+ ions in the bulk will favour the forward reaction of the reaction $HA \leftrightarrow H^+ + A^-$; consequently, there will be an enhanced ionization and hence enhanced charging of a grafted PE molecule. This enhanced charging ensures an enhanced magnitude of the EDL electrostatic potential; consequently, for larger pH_∞, $\bar{\psi}$ demonstrates a more enhanced magnitude at a given transverse location and for a given pK_a [see Figure 2.2(a)]. On the contrary, an enhanced pK_a will imply a smaller value of the ionization constant K_a (of the acid HA), which in turn will lower the concentration of A^- and hence lower the charging of the PE layer. As a result for larger pK_a, $\bar{\psi}$ shows a reduced value for a given pH_∞ and for a given transverse location [see Figure 2.2(a)]. It is worthwhile to note that there is a finite electrostatic potential

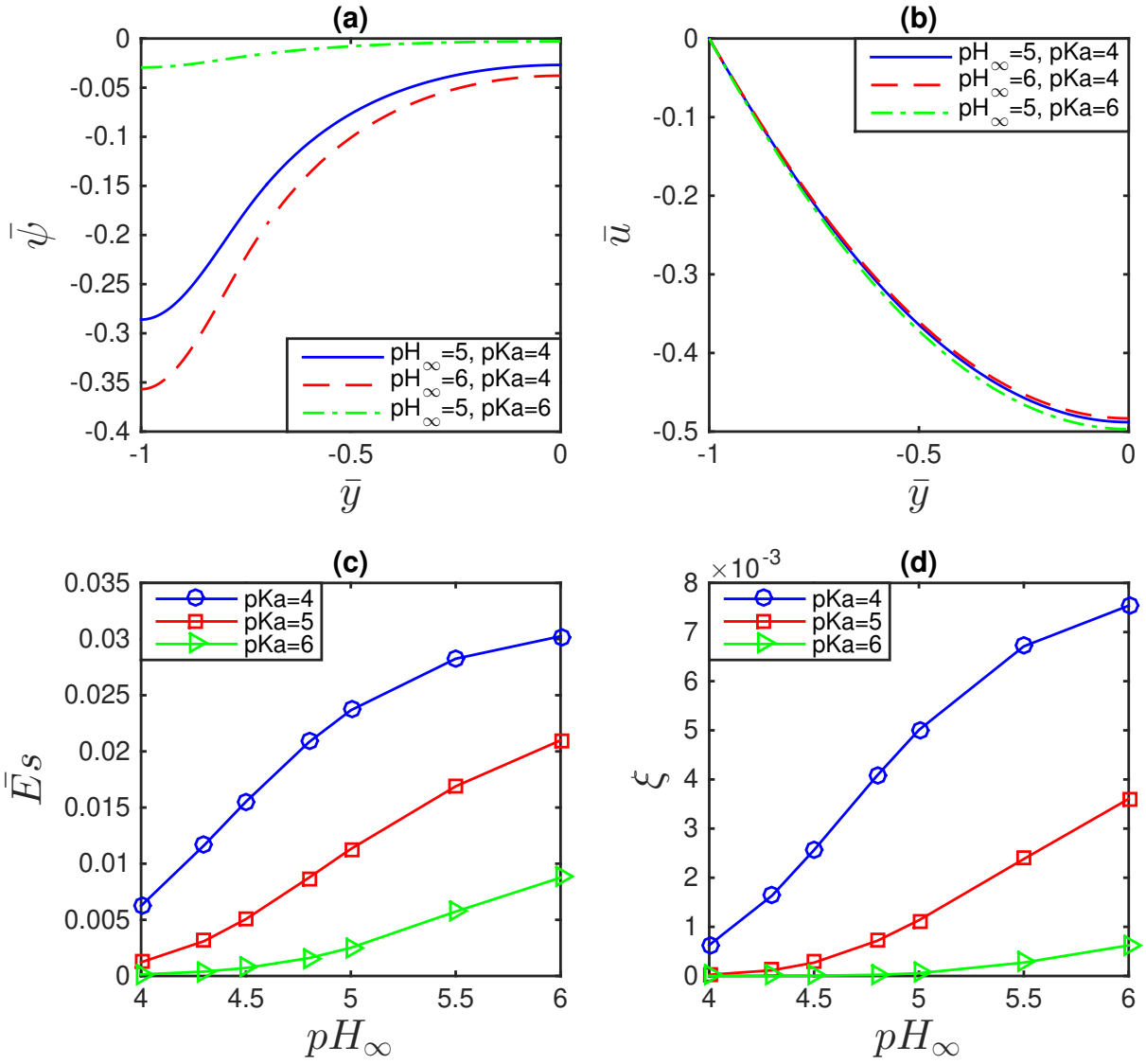

Figure 2.2: *Transverse variation of (a) dimensionless electrostatic potential* $\bar{\psi}$ *and (b) dimensionless velocity field* $\bar{u}$ *for different values of* pK_a *and* pH_∞*. Variation of (c) dimensionless streaming electric field* $\bar{E}_S$ *and (d) electrochemomechanical energy conversion efficiency* ξ *with* pH_∞ *for different values of* pK_a*. For all plots we use* $h = 100nm$*,* $c_\infty = 10^{-4}M$ *(note* $n_\infty = 10^3 N_A c_\infty$*, where* N_A *is the Avogadro number),* $\bar{d} = 0.3$*,* $\gamma_a = 0^{-4}M$*,*$u_r = 1$*,* $\alpha = 1$*,* $R_i = 1$*, and* $Na^3\sigma/d = 1$*.*

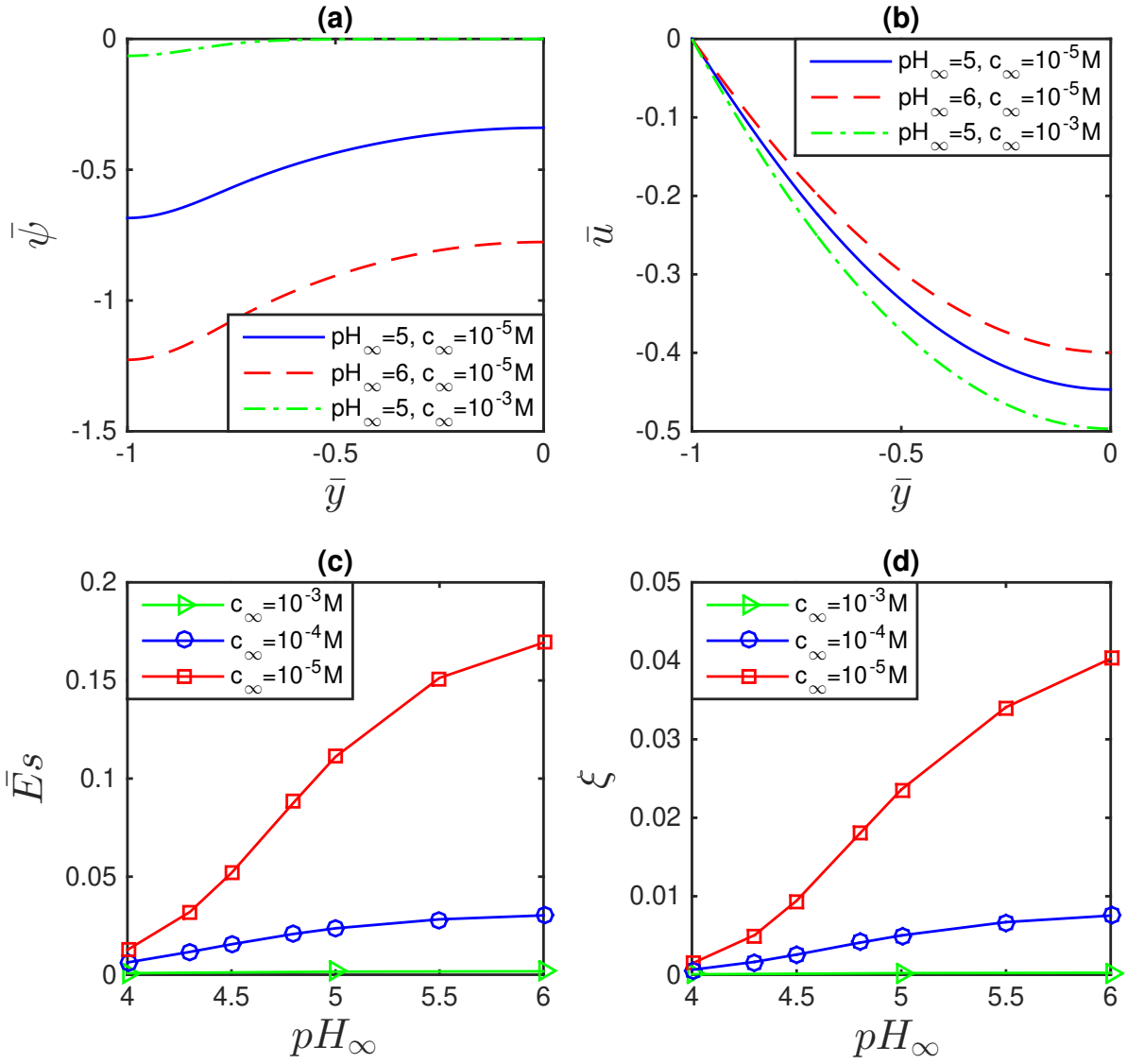

Figure 2.3: *Transverse variation of (a) dimensionless electrostatic potential* $\bar{\psi}$ *and (b) dimensionless velocity field* $\bar{u}$ *for different values of* c_∞ *and* pH_∞*. Variation of (c) dimensionless streaming electric field* $\bar{E}_S$ *and (d) electrochemomechanical energy conversion efficiency* ξ *with* pH_∞ *for different values of* c_∞*. For all plots we use* $h = 100nm$*,* $\bar{d} = 0.3$*,* $\gamma_a = 0^{-4}M$*,*$u_r = 1$*,* $\alpha = 1$*,* $pKa = 4$*,* $R_i = 1$*, and* $Na^3\sigma/d = 1$*.*

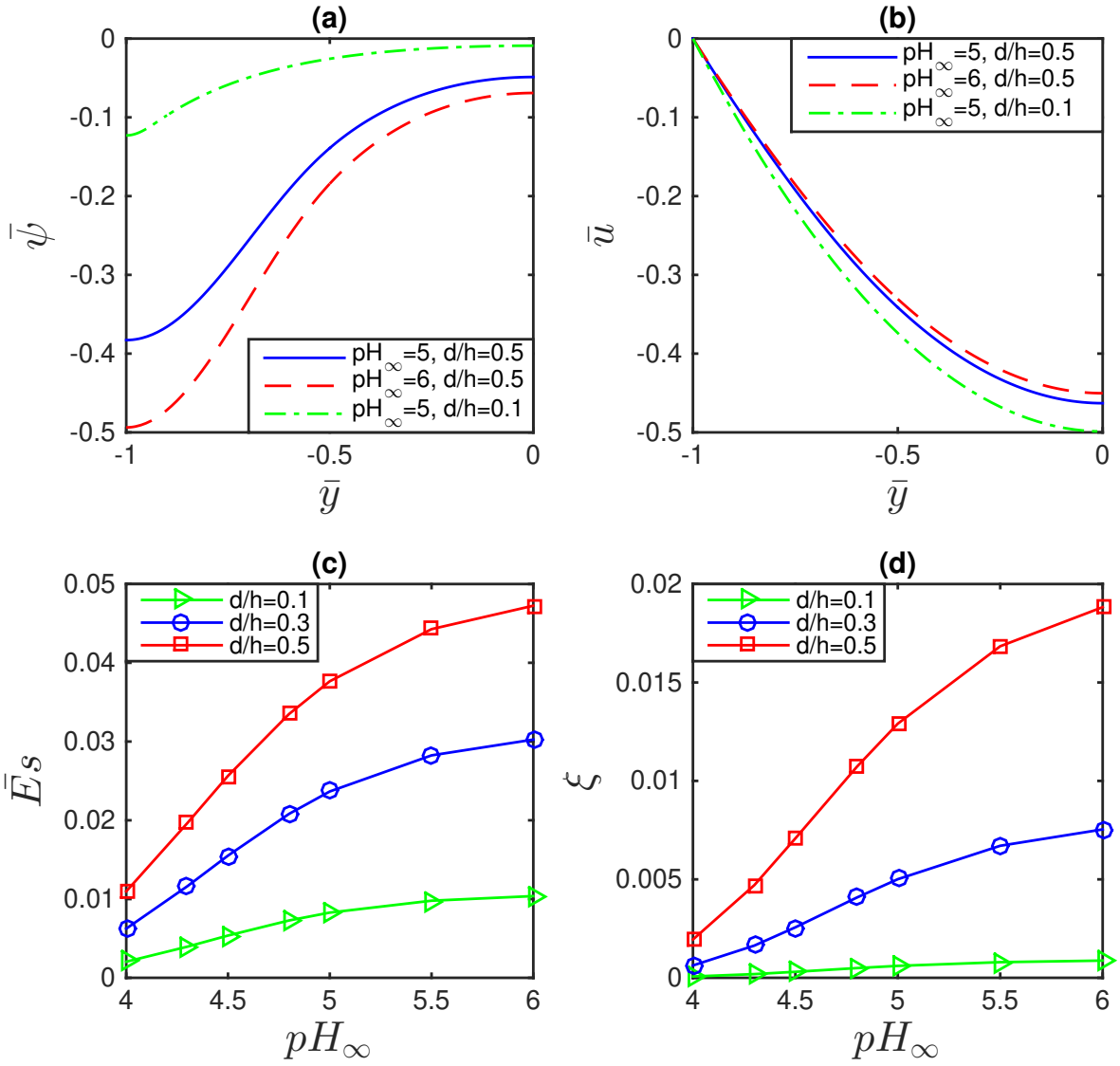

Figure 2.4: *Transverse variation of (a) dimensionless electrostatic potential* $\bar{\psi}$ *and (b) dimensionless velocity field* $\bar{u}$ *for different values of* $\bar{d} = d/h$ *and* pH_∞*. Variation of (c) dimensionless streaming electric field* $\bar{E}_S$ *and (d) electrochemomechanical energy conversion efficiency* ξ *with* pH_∞ *for different values of* c_∞*. For all plots we use* $h = 100nm$*,* $c_\infty = 10^{-4}$ M*,* $\gamma_a = 0^{-4}M$*,* $u_r = 1$*,* $\alpha = 1$*,* $pKa = 4$*,* $R_i = 1$*, and* $Na^3\sigma/d = 1$*.*

at the channel centreline for all values of for pH_∞ and d/h. This stems from the fact that the corresponding EDL thickness (λ) is $\sim 30\ nm$ (since $c_\infty = 10^{-4}$); hence $\lambda/h \approx 1/3$, ensuring significant (though weak) value of the electrostatic potential at the channel centreline. For weak values of electrostatic potentials ($|\bar{\psi}| < 1$ or $|\bar{\psi}| \sim 1$), increase in the electrostatic potential enhances the streaming current. This stems from the fact that for such ranges of the electrostatic potential, increase in the counterion concentration caused by an increase in the magnitude of the electrostatic potential invariably increases the streaming electric field. [48, 49] For larger values of the electrostatic potentials ($|\bar{\psi}| \gg 1$), the enhancement of counterion concentration (on account of increase of the electrostatic potential) may lead to a more pronounced enhancement of the conduction current, which in turn may decrease the streaming electric field. [48, 49] In the present case, $|\bar{\psi}|$ is substantially small; as a consequence, increase in $|\bar{\psi}|$ increases $\bar{E}_S$. Hence we witness an increase in $\bar{E}_S$ with an increase in pH_∞ and a decrease in pK_a [see Figure 2.2(c)]. Therefore, enhancement of $\bar{E}_S$ with pH_∞ is caused by an enhanced charging (for reasons already discussed) of the PE layer and an equivalent enhanced magnitude of the electrostatic potential. Of course, such pH_∞-dependent enhancement in $\bar{E}_S$ is witnessed only when the corresponding H^+ ion concentration is comparable to the corresponding electrolyte ion concentration; therefore, we find [see Figure 2.2(c)] at larger pH_∞ (=6) $\bar{E}_S$ starts to saturate and shows relatively weak increase with pH_∞. Enhanced magnitude of the streaming electric field will lead to a larger magnitude of the electroosmotic transport opposing the pressure-driven flow field; consequently, the magnitude of $\bar{u}$ is smaller at a given transverse location for a larger pH_∞ and smaller pK_a [see Figure 2.2(b)]. Please note

that here $\bar{u} = u/u_{p,0} < 0$ implies a positive value of u, since $u_{p,0}$ is negative [see below eq.(2.16) for the definition of $u_{p,0}$] This is commensurate with $\bar{E}_S = E_S/E_0 > 0$, which implies $E_S < 0$, since $E_0 < 0$ [see below eq.(2.16) for the definition of E_0]. Finally, in Fig. 2(d), we show the variation of the electrochemomechanical energy conversion efficiency ξ; enhancement of ξ with an increase in pH_∞ and a decrease in pK_a follows directly from the corresponding variation of the streaming current and the streaming electric field.

Figure 2.3 provides the pH and the electrolyte concentration (c_∞) dependence of the $\bar{E}_S$ and ξ. The pH dependence has already been discussed in details. Weaker concentration of the electrolyte salt leads to a more enhanced value of the EDL thickness λ, since $\lambda \propto 1/\sqrt{c_\infty}$. Enhanced λ will imply a weaker screening of the EDL electrostatic potential (on either sides of the PE-layer-EDL interface), thereby ensuring an enhanced magnitude of $\bar{\psi}$ for a smaller c_∞ value [see Figure 2.3(a)]. This also implies a much larger magnitude of the channel centreline electrostatic potential for smaller c_∞. Consequently, following the discussions provided for Figure 2.2, we may infer that an enhanced c_∞ leads to an enhanced $\bar{E}_S$ [for a given pH_∞, see Figure 2.3(c)], a weakened magnitude of $\bar{u}$ [for a given transverse location and for a given pH_∞, see Figure 2.3(b)], and an enhanced electrochemomechanical energy conversion efficiency [for a given pH_∞, see Figure 2.3(d)].

Finally, Figure 2.4 shows the effect of the pH and the PE layer thickness on $\bar{E}_S$ and ξ. Enhanced $\bar{d} = d/h$ (or PE layer thickness) will imply larger number of the PE charges, which in turn will lead to a larger value of $\bar{\psi}$ [see Figure 2.4(a)]. Such dependence of $\bar{\psi}$ on $\bar{d}$ has been previously reported by us. [13] Such enhanced

$\bar{\psi}$ ensures that increase in $\bar{d}$ enhances $\bar{E}_S$ [for a given pH_∞, see Figure 2.4(c)], lowers the magnitude of $\bar{u}$ [for a given transverse location and for a given pH_∞, see Figure 2.4(b)], and increases the electrochemomechanical energy conversion efficiency [for a given pH_∞, see Figure 2.4(d)].

Comparison of Figures 2.2-2.4 will allow selection of the appropriate parameter space that will enable electrochemomechanical energy conversion of maximum efficiency. We find that we obtain a efficiency value of around $4-5\%$ for optimal choices of system parameters [e.g., please see Figure 2.4(d)]. This is a significantly high number given the 3% efficiency value reported in pioneering experiments of Daiguji et al. [36] We shall like to mention here that our results should not be compared with the several theoretical results that report an efficiency of nearly 100%. [55, 56] The reason is that these high efficiency values result from erroneous definition of the input power, where the input velocity is considered as the velocity reduced due to the impact of the streaming electric field.

Our theoretical calculations proposed here can be used to show that by pumping a weak acid electrolyte solution ($c_\infty = 10^{-5}M$ and $pH = 6$) with 5 bar pressure continuously into PE-grafted nannochannels (with the channel height of $h = 100nm$) that constitute a 1cm×1cm porous material (with the thickness of 1mm and a high porosity ratio of 60%), a 5 watt electrical power (sufficient to light up an LED lamp) can be generated, provided the supposed technical issues related to e.g. electrode polarization and pressure resistance can be overcome.

2.4 Discussions

2.4.1 Comparison with experimental results

We compare our theoretical predictions with the experimental results of Zimmerman, Duval and co-workers. [23,57,58] These comparisons also provide a validity of our proposed theoretical model. Comparisons are done for the variation of the streaming current (i_S) as a function of the pH and the salt concentration. While we do not attempt a direct quantitative comparison, we do find the exact same trend in the theoretical prediction of i_S as compared to the experimental findings. For example, our theory predicts first an increase and then a saturation in i_S with an increase in salt concentration for a given pH and given a pK_a [see Figure 2.5(a)]. Exactly similar findings are obtained from the experiments on streaming currents conducted at the interfaces grafted with poly(ethylene oxide) or PEO brushes and a hydrogel layer. Our theory also predicts a monotonic increase in the magnitude of the negative value of i_S with pH (pH always in the acidic range and not too small) [see Figure 2.5(b)]. Qualitatively exactly similar results are obtained from experiments on interfaces grafted with PEO brushes.

2.4.2 Comparison with findings of existing theoretical studies

It is worthwhile to compare the findings of this study in light of the results from the existing theoretical studies. [23,24,57–60] There are several aspects in which this study and its results are distinct in comparison to that of the existing similar

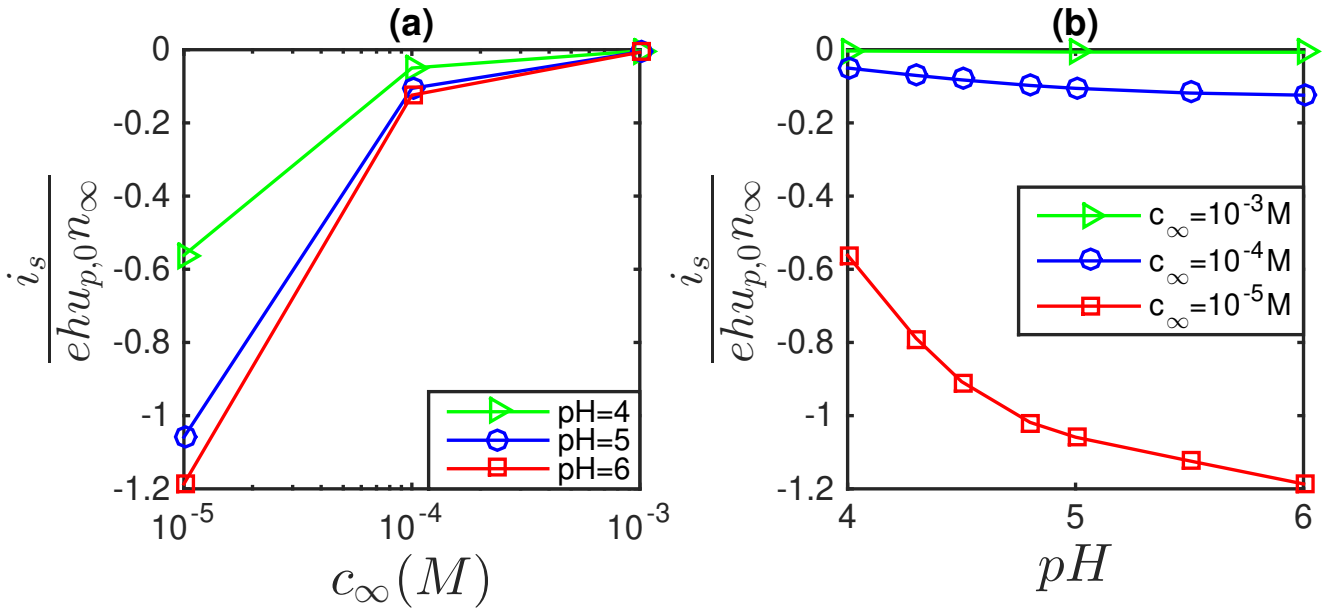

Figure 2.5: *Variation of the dimensionless streaming current with (a) c_∞ for different values of c_∞ and (b) c_∞ for different values of pH_∞. Other parameters are same as that of Fig. 3. These results, obtained using our theoretical model, allows to compare our theoretical predictions with respect to the existing experiments.*

theoretical calculations. First and foremost, the analysis in this study is unique in the sense it solves an integro-differential equation to obtain the nanochannel streaming potential. Such an approach has only been used once ever before in one of our previous studies. [19] Secondly, the calculations are provided for nanochannels; therefore PE brushes are nanoconfined PE brushes, which are unlike the PE brushes grafted to single interfaces [57] or surfaces of microchannels. [23, 24, 60] Thirdly, we provide results that depict the competitive interplay between pH, pK_a, ion concentration and PE brush thickness relative to the nanoconfinement in the overall variation of the streaming potential. Such explicit roles of pK_a and relative thickness of the PE brushes have rarely been identified in context of nanoscale streaming potential in soft nanochannels. Finally, we provide the energy conversion efficiency in such pH-responsive soft nanochannels; such a thing has also never been reported previously.

2.4.3 Selection of the thickness of the PE brush layer: Choice of cubic monomer profile

One of the key issues associated with the PE or polymer brushes is the selection of the appropriate monomer distribution. This distribution depends on the nature of the polymer or PE chain, the nature of the solvent, the concentration of the polymer in the solvent, etc. Nature of the polymer chain dictates whether or not one can neglect the chain correlations. For cases where such correlations cannot be neglected, a self-consistent-field-theory (SCFT) has been proposed for uncharged polymer chains yielding quadratic profile for the monomer distribution for mono-disperse chains [61,

62] and a deviation from this quadratic profile for poly-disperse chains (with the poly-dispersity being triggered by the presence of heterogeneities in the chain lengths). [57, 63] While this self-consistent field theory is the most appropriate representation of the brush monomer profile, it suffers from a key limitation. This limitation is that either of these two profiles (quadratic or the profile that is slightly deviated from it) is based on the assumption that the correlations between the polymer chain segments is represented as binary collisions. Therefore this simplistic profile is not an appropriate representation of the case where the polymer contains backbone charges (i.e., it is a PE), triggering an EDL-mediated interaction between the segments. In fact, it is rather recently that there have been attempts to study the profiles of PE brushes using this SCFT framework with appropriate consideration of the PE charges and the resulting EDL ion distribution. [64–67] However, barring only one study by Witte et al., [64] virtually none of these studies account for pH-dependent charge density of the PE brushes. Also this study by Witte et al. does not provide the explicit variation of the monomer density profile as a function of pH, neither does it account for the pH-dependent charging explicitly in expressing the electrostatic contribution of the PE charge in the overall Hamiltonian. These limitations of the SCFT can be typically associated with the extreme complexities of the governing equations that necessitate employing an extremely tedious numerical approach, often forbidding the incorporation of novel physical issues associated with the nature of charging of the PE.

A much more tractable and simplified approach involves cases where one disregards the correlation effects between the segments of the PE brush. Such a situation

is possible if one considers the PE brushes as Gaussian chain (where there are no chain-chain correlations) or operates in a specified phase space where these correlations can be neglected even for real chains. [61, 68, 69] For such cases, an analytically tractable mean field approach, often known as the Strong stretching Theory or SST, is proposed by the works of Zhulina and co-workers. [10, 39, 40] This approach proposes a monomer density profile of the form $\sqrt{A + By^2} + C$ for uncharged polymer brushes. [10] Of course, this approach allows for a much easy incorporation of the PE charge, effect of pH-dependence of this charge, and the resulting distribution of the electrolyte ions forming the EDL. Typical monomer density profiles are combinations of quadratic and exponential profiles. [40] A simplified version of this model by Zhulina and co-workers is the well-known Scheutjens-Fleer model [70, 71] that substantially simplifies the description of the EDL electrostatics by resorting to replace the Poisson-Boltzmann description by a description based on the net electroneutrality of the system. Therefore, the expected state of the art in modelling the monomer distribution of grafted PE brushes is either the more rigorous (and only tractable numerically) SCFT for PE chains (that may not be suitable to unravel the impact of pH-dependent PE charge density on the monomer profile), or the more tractable SST that seems more apt to incorporate the specifics of pH-dependence of PE charge density.

Given that we are interested to analyze the case of PE brushes with pH-dependent charge density, it is more logical to focus on the SST theory of Zhulina and co-workers, since this is the only existing mean field theory that has so far been able to quantify the effect of pH-dependent charge density on the overall monomer

distribution. [40] In our recent study, [16] we discovered a major issue with the SST theory in context of modelling the electrostatics for the case of PE brushes with pH-dependent charge density. It stemmed from the fact that the hydrogen ion distribution was always assumed to obey Boltzmann distribution both inside and outside the PE layer. As we demonstrated in theory section as well as in the detailed derivation in the Appendix section, such a consideration is incorrect and provides an energetically inconsistent picture, since the free energy is not minimized with respect to H^+ ion concentration. We did this minimization with respect to H^+ ion concentration; these new equations are the appropriate free energy representation of the problem, since the free energy has been minimized with respect to all the governing variables. Now the resulting equations are such that they need to be coupled with a particular kind of monomer distribution $\varphi(y)$ that simultaneously ensure the four conditions illustrated in eqs.(12,13); this is possible with the *non-unique* cubic monomer profile.

There is a major assumption in our analysis (which yields this cubic monomeric distribution). This assumption is that the PE thickness is independent of the electrostatic effects. This is possible when $\Delta F_{PE,elec} \gg \left(\Delta F_{PE,ent} + \Delta F_{PE,EV}\right)$, or $\Delta F_{PE,elec} \ll \left(\Delta F_{PE,ent} + \Delta F_{PE,EV}\right)$. Under such conditions (satisfied by $\sigma \ll 1/(at)$ or $\sigma \gg 1/(at)$, where σ is the grafting density, a is the PE Kuhn length, t is the PE thickness), [1] the electrostatic energy of the PE brush and the resulting EDL balances each other, and this in turn dictates the electrostatics of the problem. Therefore, this cubic monomer distribution is the distribution of the chargeable sites of the PE brushes. This implies that if we have a situation where $\Delta F_{PE,elec} \gg \left(\Delta F_{PE,ent} + \Delta F_{PE,EV}\right)$ or $\Delta F_{PE,elec} \ll \left(\Delta F_{PE,ent} + \Delta F_{PE,EV}\right)$ and the PE exhibits

a pH-dependent charge density, the PE chargeable sites must demonstrate a *non-unique cubic distribution*. It is evident that this is a simplified approach. A more rigorous approach should necessitate solution of the SST considering the elastic, excluded volume, and electrostatic energy of the PE brush molecule as well as the EDL energy with the consideration of explicit H^+ ions (or in other words, the free energy should be minimized with respect to the H^+ ion number density distribution). Such a formulation is missing in the existing literature, and we plan to take it up in a future problem. Of course, the ultimate calculation should be the SCFT modelling (with finite correlation effects) of the PE brush molecule with explicit consideration of the H^+ ions. Such a step will provide the final answer in context of the configuration and the monomer distribution of a PE brush with pH-dependent charge density.

2.5 Conclusion

In this paper, we provide a theory to calculate the streaming electric field and the efficiency of the resulting electrochemomechanical energy conversion in a nanochannel grafted with a PE molecules with pH-dependent charge density. Our analyses, based on appropriate free energy description of the problem as well as solution of a rigorous integro-differential equation, provide new insights to the role of the bulk pH and the pK_a of the dissociating acid (which charges the PE layer) in the streaming electric field and the energy conversion. We establish that the energy conversion efficiency can be substantially high ($\sim 4-5\%$) for optimum parameter choices; this finding emboldens our previous studies, [13, 19] and establishes PE-grafted nanochannels as

efficient nanfluidic electrochemomechanical energy converted under most practical conditions.

.1 Appendix: Derivation of the governing equations

The free energy can be expressed as:

$$\Delta F' = \int \Delta f \left[\psi, n_{\pm}, n_{H^+}, n_{OH^-}\right] d^3\mathbf{r}, \tag{.1.1}$$

where Δf is the free energy density, expressed as (written in expanded form and using eq.(6) to express n_{A^-}):

$$\Delta f = -\frac{\epsilon_0\epsilon_r}{2}|\nabla\psi|^2 + e\psi(n_+ - n_-) + e\psi(n_{H^+} - n_{OH^-}) - e\frac{K'_a\gamma_a\varphi}{K'_a + n_{H^+}}\psi$$
$$+k_BT[n_+(\ln(\frac{n_+}{n_{+,\infty}}) - 1) + n_-(\ln(\frac{n_-}{n_{-,\infty}}) - 1) + n_{H^+}(\ln(\frac{n_{H^+}}{n_{H^+,\infty}}) - 1)$$
$$+n_{OH^-}(\ln(\frac{n_{OH^-}}{n_{OH^-,\infty}}) - 1)] \qquad [\text{for} \quad -h \le y \le -h + d],$$

$$\Delta f = -\frac{\epsilon_0\epsilon_r}{2}|\nabla\psi|^2 + e\psi(n_+ - n_-) + e\psi(n_{H^+} - n_{OH^-}) + k_BT[n_+(\ln(\frac{n_+}{n_{+,\infty}})$$
$$-1) + n_-(\ln(\frac{n_-}{n_{-,\infty}}) - 1) + n_{H^+}(\ln(\frac{n_{H^+}}{n_{H^+,\infty}}) - 1) + n_{OH^-}(\ln(\frac{n_{OH^-}}{n_{OH^-,\infty}}) - 1)].$$
$$[\text{for} \quad -h + d \le y \le 0]$$

The equilibrium conditions will be obtained by minimizing eq.(.1.2) with respect to ψ, n_+, n_-, n_{H^+}, n_{OH^-}. Below we discuss this minimization procedure in details.

Minimizing with respect to ψ yields:

$$\frac{\delta(\Delta F')}{\delta\psi} = 0 \Rightarrow \frac{\partial(\Delta f)}{\partial\psi} - \frac{d}{dy}\left(\frac{\partial(\Delta f)}{\partial\psi'}\right)$$
$$\Rightarrow \frac{d^2\psi}{dy^2} = \frac{-e(n_+ - n_-) + e\frac{K'_a\gamma_a\varphi}{K'_a+n_{H^+}} - e(n_{H^+} - n_{OH^-})}{\epsilon_0\epsilon_r}$$
$$[\text{for} \quad -h \le y \le -h+d],$$

$$\frac{\delta(\Delta F')}{\delta\psi} = 0 \Rightarrow \frac{\partial(\Delta f)}{\partial\psi} - \frac{d}{dy}\left(\frac{\partial(\Delta f)}{\partial\psi'}\right)$$
$$\Rightarrow \frac{d^2\psi}{dy^2} = \frac{-e(n_+ - n_-) - e(n_{H^+} - n_{OH^-})}{\epsilon_0\epsilon_r} \tag{.1.2}$$
$$[\text{for} \quad -h+d \le y \le 0].$$

Minimizing with respect to $n_\pm$ yields:

$$\frac{\delta(\Delta F')}{\delta n_\pm} = 0 \Rightarrow n_\pm = \left(n_{\pm,\infty}\right)\exp\left(\mp\frac{e\psi}{k_BT}\right) \qquad [\text{for} \quad y \ge -h]. \tag{.1.3}$$

Minimizing with respect to n_{OH^-} yields:

$$\frac{\delta(\Delta F')}{\delta n_{OH^-}} = 0 \Rightarrow n_{OH^-} = \left(n_{OH^-,\infty}\right)\exp\left(\frac{e\psi}{k_BT}\right) \ [\text{for} \quad y \ge -h]. \tag{.1.4}$$

Minimizing with respect to n_{H^+} yields:

$$\frac{\delta(\Delta F')}{\delta n_{H^+}} = 0 \Rightarrow n_{H^+} = \left(n_{H^+,\infty}\right)\exp\left[-\frac{e\psi}{k_BT}\left(1 + \frac{K'_a\gamma_a\varphi}{\left(K'_a + n_{H^+}\right)^2}\right)\right]$$
$$[\text{for} \quad -h \le y \le -h+d],$$
$$\frac{\delta(\Delta F')}{\delta n_{H^+}} = 0 \Rightarrow n_{H^+} = \left(n_{H^+,\infty}\right)\exp\left(-\frac{e\psi}{k_BT}\right)$$
$$[\text{for} \quad -h+d \le y \le 0]. \tag{.1.5}$$

Eqs. (7-9) are the dimensionless forms of eqs.(.1.3,.1.4,.1.5). Eq.(.1.5) establishes that n_{H^+} distribution within the PE layer deviates from that predicted by the Boltzmann partitioning. This stems from the fact that the pH-dependent charge density of the

PE induces a particular kind of n_{H^+}-dependent term in the free energy functional. In virtually all the previous studies on mean field modelling of the electrostatics of grafted PE layer with pH-dependent PE charge density, while this term was included in the free energy density, the hydrogen ion equilibrium was not obtained by minimizing this free energy density with respect to n_{H^+}; rather in a most ad hoc and erroneous fashion it was assumed to obey the Boltzmann distribution. Please note that we do recover the Boltzmann distribution for H^+ ion concentration outside the PE layer and for OH^- ion in the entire system. Of course, we shall have OH^- ions deviating from Boltzmann distribution for cases where the PE is positively charged and demonstrate a pOH-dependent charge density; for that case the H^+ ion will obey the Boltzmann distribution in the entire system. To summarize, therefore, this deviation of H^+ ion concentration from the Boltzmann distribution occurs by virtue of the fact that the PE layer demonstrate pH-dependent charging, and the equilibrium H^+ ion concentration *must* be obtained (something that, most erroneously, has not been done by other researchers) from minimization of the free energy change with respect to n_{H^+}.

Chapter 3: Electrokinetics in nanochannels grafted with poly-zwitterionic brushes

In this chapter,[1] *the electrokinetic transport in soft nanochannels grafted with poly-zwitterionic (PZI) brushes. The transport is induced by an external pressure gradient, which drives the ionic cloud (in the form of an electric double layer or EDL) at the brush surfaces to induce an electric field that drives an induced electroosmotic transport. We characterize the overall transport by quantifying this electric field, overall flow velocity, and the energy conversion associated with the development of the electric field and a streaming current. We specially focus on how the ability of the PZI to ionize and demonstrate a significant charge at both large and small pH can be efficiently manoeuvred to develop a liquid transport, an electric field, and an electrokinetically induced power across a wide range of pH values.*

[1]Contents of this chapter have been published as: *G. Chen, J. Patwary, H. S. Sachar, and S. Das, Electrokinetics in nanochannels grafted with poly-zwitterionic brushes. Microfluid. Nanofluid. (Submitted)*

3.1 Introduction

Functionalizing nanoscale interfaces (e.g., walls of a nanochannels or the surfaces of nanoparticles) with polymer and polyelectrolyte (PE) brushes [2–6, 33] have been extensively used for a myriad of applications such as targeted drug delivery [72, 73], oil recovery [74], ion and biosensing [75–79], current rectification [80], fabrication of nanofluidic diodes [81, 82] and nanoactuators [83], and many more. The central idea that drives most of these applications is how the brushes respond to the environmental stimuli (e.g., local pH, salt concentration, temperature, etc.) and regulate the transport of different species. Under these conditions, there have been significant efforts in studying the ion and liquid transport in nanochannels or nanopores grafted with PE brushes that are pH-responsive [1, 18, 41, 75, 76, 84–95].

Polyzwitterion (PZI) is a particular type of PE that contains both negative and positive sites [96]. These sites typically ionize as a function of the local pH; however, the extent of ionization of the positive and the negative sites are different at different pH. Therefore, at a given pH the PZI is either negatively or positively charged. The PZI molecules have been extensively employed in a large number of applications, such as the fabrication of "smart" materials with environmental-stimuli-responsive switchable properties [97], sub-surface imaging and oil recovery [98], capturing chemical moieties [99], drug delivery [100], biomacromolecular separation [101], removal of organic pollutants [102], use as heterogeneous catalysts [103], and many more. In this paper, we study the electrohydrodynamics in a nanochannel grafted with such PZI molecules existing in a "brush" like state. There have been significant previous

efforts where interfaces grafted with such PZI brushes have been used for a variety of applications such as triggering extreme lubrication [104, 105], reversible switching of the surface wettability [106, 107], inducing repeatable adhesion [108], fabrication of anti-fouling surfaces [109], regulating ion selectivity in nanopores [110], etc. But this is for the first time that its effect in electrohydrodynamics and electrokinetic energy conversion in a brush-grafted nanochannel is being probed.

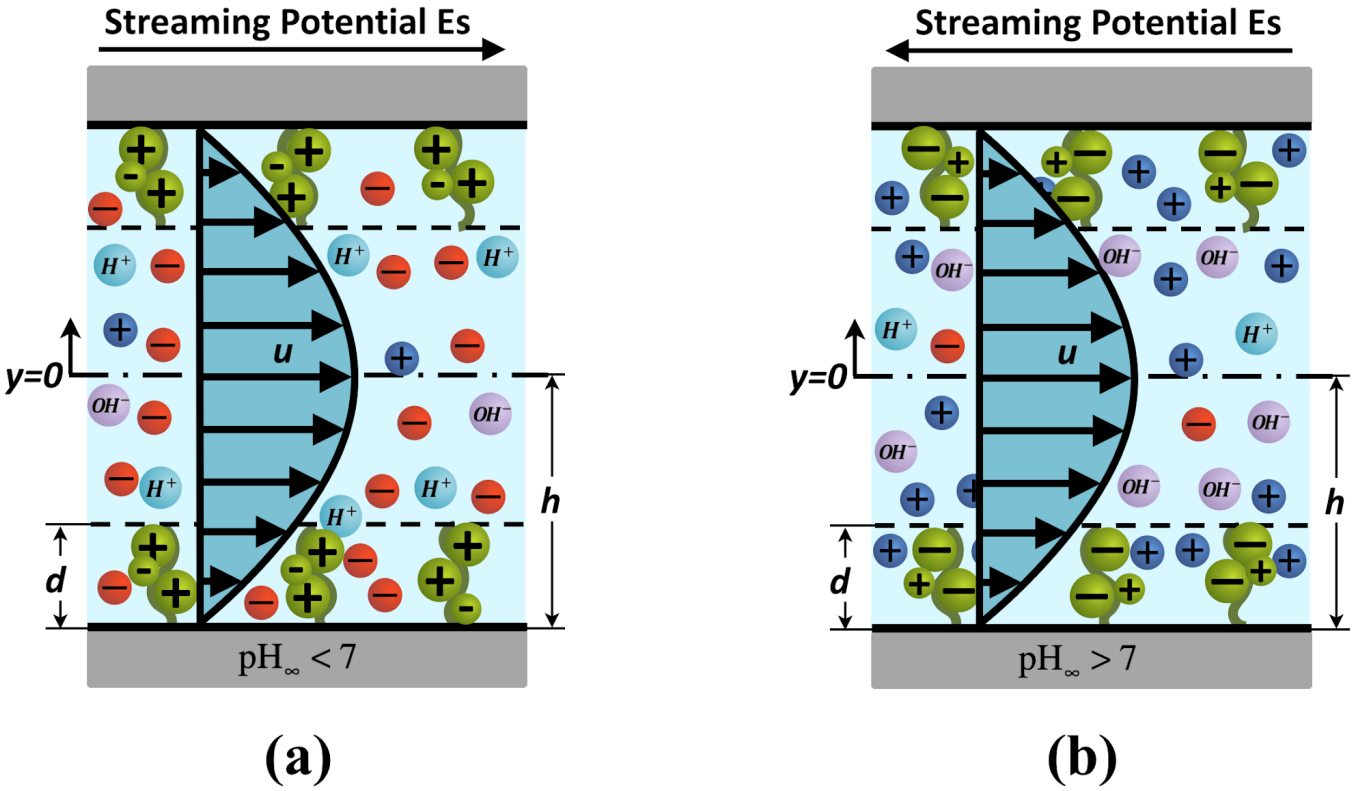

Figure 3.1: *Schematic showing the pressure-driven transport and induced electric field in a PZI-brush grafted nanochannels. The PZI brush is positively charged for small pH ($pH_\infty < 7$) [see (a)] and negatively charged for large pH ($pH_\infty > 7$) [see (b)], leading to the generation of a positive streaming potential [see (a)] and a negative streaming potential [see (b)].*

Our paper provides detailed calculations of the pH-responsive electric double layer electrostatics and how that electrostatics regulates the flow and the overall electrokinetics in presence of an externally imposed pressure-driven transport. We calculate the electric field induced by this pressure-driven transport and how this electric field and the induced streaming current couple to generate an electrokinetic power. This power generation is an example of electrochemomechanical energy conversion and has been touted as one of the key applications of nanochannel electrokinetic transport [13, 19, 36, 37, 84, 111–113]. Here we establish that working with the PZI brush allows for the generation of the large electrokinetic power across a wide range of pH (i.e., for both large and small pH). In other words, this paper points to a new design information in the context of electrokinetic power generation in soft or PE-brush-grafted nanochannels – a single design allows the flexibility of generating electrokinetic power across a wide spectrum of pH, which is not possible for brush-free nanochannels [36, 37, 112, 113] or nanochannels grafted with the PE (and not PZI) brushes [84].

3.2 Theory

3.2.1 Electrostatics

We consider a pressure-driven transport in a nanochannel of height $2h$ and grafted with a layer of PZI brushes of constant height d (with $d < h$) (see Figure 3.1). In order to obtain the overall transport, we would have to first get the electrostatics of the EDL induced by the brushes. Considering the bottom half of a nanochannel

(i.e., $-h \leq y \leq 0$), the free energy functional dictating the EDL electrostatics can be expressed as:

$$\mathcal{F} = \int f\left[\psi, n_{\pm}, n_{H^+}, n_{OH^-}\right] d^3\mathbf{r}, \tag{3.1}$$

where ψ is the electrostatic potential, n_i is the number density of the ion i ($i = \pm, H^+, OH^-$) and f is the free energy density expressed as:

$$f = k_B T[n_+(\ln(\frac{n_+}{n_{+,\infty}}) - 1) + n_-(\ln(\frac{n_-}{n_{-,\infty}}) - 1) + n_{H^+}(\ln(\frac{n_{H^+}}{n_{H^+,\infty}}) - 1)$$
$$+ n_{OH^-}(\ln(\frac{n_{OH^-}}{n_{OH^-,\infty}}) - 1)] - \frac{\epsilon_0\epsilon_r}{2}|\nabla\psi|^2 + e\psi(n_+ - n_- + n_{H^+} - n_{OH^-} - \varphi n_{A^-} + \varphi n_{BH^+})$$
$$[\text{for} \quad -h \leq y \leq -h + d],$$

$$f = k_B T[n_+(\ln(\frac{n_+}{n_{+,\infty}}) - 1) + n_-(\ln(\frac{n_-}{n_{-,\infty}}) - 1) + n_{H^+}(\ln(\frac{n_{H^+}}{n_{H^+,\infty}}) - 1)$$
$$+ n_{OH^-}(\ln(\frac{n_{OH^-}}{n_{OH^-,\infty}}) - 1)] - \frac{\epsilon_0\epsilon_r}{2}|\nabla\psi|^2 + e\psi(n_+ - n_- + n_{H^+} - n_{OH^-}) \tag{3.2}$$
$$[\text{for} \quad -h + d \leq y \leq 0].$$

In eq.(3.2), $k_B T$ is the thermal energy, e is the electronic charge, ϵ_0 is the permittivity of free space, ϵ_r is the relative permittivity of the medium, e is the electronic charge, $n_{i,\infty}$ is the bulk number density of the ions i ($i = \pm, H^+, OH^-$) and φ is the dimensionless distribution of the PZI chargeable sites (PZICS) of a given brush molecule. The brush being a PZI brush, the PZICS will simultaneously consist of a negative charge centre and a positive charge centre. The formation of the negative charge centre can be attributed to the ionization of an acidic functional group HA ($HA \leftrightarrow H^+ + A^-$; ionization constant K_a having the units of $moles/liter$) yielding A^- ions. On the other hand, the formation of the positive charge centre can be attributed to the ionization of a basic functional group B ($B + H_2O \leftrightarrow BH^+ + OH^-$;

ionization constant K_b having the units of $moles/liter$) yielding BH^+ ions. Under these conditions the number densities (in units of $1/m^3$) of the ionic groups of the PZI molecule (namely n_{A^-} and n_{BH^+}) can be expressed as:

$$n_{A^-} = \frac{K'_a \gamma_a}{K'_a + n_{H^+}}, \tag{3.3}$$

$$n_{BH^+} = \frac{K'_b \gamma_b}{K'_b + n_{OH^-}}, \tag{3.4}$$

where γ_a and γ_b are the maximum site densities of acidic and basic functional groups of the PZI, $K'_a = 10^3 N_A K_a$, and $K'_b = 10^3 N_A K_b$ (N_A is the Avogadro number). Of course eqs.(3.2-3.4) show the dependence of the overall problem on the pH of the system.

The equilibrium electrostatic potential and the concentration distribution of different ions can be obtained by minimizing $\mathcal{F}$. Minimizing $\mathcal{F}$ with respect to ψ, we get (considering only the bottom half of the nanochannel):

$$\frac{\delta \mathcal{F}}{\delta \psi} = 0 \Rightarrow \frac{\partial f}{\partial \psi} - \frac{d}{dy}\left(\frac{\partial f}{\partial \psi'}\right) \Rightarrow \frac{d^2\psi}{dy^2} = \frac{e\left(n_- - n_+ + n_{OH^-} - n_{H^+} + \varphi n_{A^-} - \varphi n_{BH^+}\right)}{\epsilon_0 \epsilon_r}$$

$$[\text{for} \quad -h \leq y \leq -h + d],$$

$$\frac{\delta \mathcal{F}}{\delta \psi} = 0 \Rightarrow \frac{\partial f}{\partial \psi} - \frac{d}{dy}\left(\frac{\partial f}{\partial \psi'}\right) \Rightarrow \frac{d^2\psi}{dy^2} = \frac{e\left(n_- - n_+ + n_{OH^-} - n_{H^+}\right)}{\epsilon_0 \epsilon_r}$$

$$[\text{for} \quad -h + d \leq y \leq 0]. \tag{3.5}$$

Minimizing $\mathcal{F}$ with respect to $n_\pm$, n_{H^+} and n_{OH^-}, we get the expression of the ion

distributions:

$$\frac{\delta F}{\delta n_{\pm}} = 0 \Rightarrow n_{\pm} = \left(n_{\pm,\infty}\right) \exp\left(\mp \frac{e\psi}{k_B T}\right) \quad [\text{for} \quad y \geq -h], \tag{3.6}$$

$$\frac{\delta F}{\delta n_{OH^-}} = 0 \Rightarrow n_{OH^-} = \left(n_{OH^-,\infty}\right) \exp\left[\frac{e\psi}{k_B T}\left(1 + \varphi \frac{K_b' \gamma_b}{\left(K_b' + n_{OH^-}\right)^2}\right)\right] \quad [\text{for} \quad -h \leq y \leq -h + d],$$

$$\frac{\delta F}{\delta n_{OH^-}} = 0 \Rightarrow n_{OH^-} = \left(n_{OH^-,\infty}\right) \exp\left(\frac{e\psi}{k_B T}\right) \quad [\text{for} \quad -h + d \leq y \leq 0]. \tag{3.7}$$

and

$$\frac{\delta F}{\delta n_{H^+}} = 0 \Rightarrow n_{H^+} = \left(n_{H^+,\infty}\right) \exp\left[-\frac{e\psi}{k_B T}\left(1 + \varphi \frac{K_a' \gamma_a}{\left(K_a' + n_{H^+}\right)^2}\right)\right] \quad [\text{for} \quad -h \leq y \leq -h + d],$$

$$\frac{\delta F}{\delta n_{H^+}} = 0 \Rightarrow n_{H^+} = \left(n_{H^+,\infty}\right) \exp\left(-\frac{e\psi}{k_B T}\right) \quad [\text{for} \quad -h + d \leq y \leq 0]. \tag{3.8}$$

Here $n_{\pm,\infty}$ are the bulk number density of the electrolyte ions, $n_{H^+,\infty} = 10^3 N_A 10^{-pH_\infty}$ is the bulk number density of hydrogen ions (pH_∞ is the bulk pH), $n_{OH^-,\infty} = 10^3 N_A 10^{-pOH_\infty}$ (pOH_∞ is the bulk pOH) is the bulk number density of the hydroxide ions and $pH_\infty + pOH_\infty = 14$. The bulk number densities are the number densities of the ions in the microchannel reservoirs (where $\psi = 0$) connecting the nanochannel [114–116]. Solution of ψ can be obtained by first using eqs.(3.6,3.7,3.8) to replace the ion number densities appearing in eq.(3.5), and then solving the resultant differential equation in ψ in presence of the boundary conditions expressed

below:

$$(\frac{d\psi}{dy})_{y=0} = 0, \quad (\psi)_{y=(-h+d)^+} = (\psi)_{y=(-h+d)^-}, \quad (\frac{d\psi}{dy})_{y=(-h+d)^+} = (\frac{d\psi}{dy})_{y=(-h+d)^-},$$
$$(\frac{d\psi}{dy})_{y=-h} = 0. \tag{3.9}$$

The critical thing to note here is that this differential equation in ψ will also contain the unresolved expression for n_{H^+} and n_{OH^-}; this stems from the fact that while the expressions for the number densities of $n_\pm$ are explicit in ψ [see eqs.(3.6,3.7)], n_{H^+} and n_{OH^-} are implicit in ψ [see eq.(3.7,3.8)]. Therefore, we shall have a set of equations for ψ, n_{H^+}, and n_{OH^-} that will be needed to be solved simultaneously. Finally, we would like to point out that this coupled solution of ψ and n_{H^+} as well as ψ and n_{OH^-} will require the information on the distribution of $\varphi = \varphi(y)$. We shall discuss this choice of $\varphi(y)$ later.

PZI brush layer in an acidic solution

We first consider the PZI brush layer dissociation in an acidic solution. We consider that the acid furnishes the same anion as the salt. As a consequence, the bulk number density of the salt anion will be $n_\infty + n_{H^+,\infty}$. Under this condition, we can non-dimensionalize eqs.(3.7,3.8) as well as the equation that results from using

eqs.(3.6,3.7,3.8) to replace the ion number densities in eq.(3.5) to yield:

$$\begin{aligned}
\frac{d^2\bar{\psi}}{d\bar{y}^2} &= \frac{1}{2\bar{\lambda}^2}\left[\bar{n}_- - \bar{n}_+ + \bar{n}_{OH^-} - \bar{n}_{H^+} + \varphi\bar{n}_{A^-} - \varphi\bar{n}_{BH^+}\right] \qquad [\text{for} \quad -1 \le \bar{y} \le -1+\bar{d}] \\
&= \frac{1}{2\bar{\lambda}^2}\left[\left(1+\bar{n}_{H^+,\infty}\right)\exp\left(\bar{\psi}\right) - \exp\left(-\bar{\psi}\right) + \bar{n}_{OH^-} - \bar{n}_{H^+} + \varphi\frac{\bar{K}'_a\bar{\gamma}_a}{\bar{K}'_a+\bar{n}_{H^+}} - \varphi\frac{\bar{K}'_b\bar{\gamma}_b}{\bar{K}'_b+\bar{n}_{OH^-}}\right], \\
\frac{d^2\bar{\psi}}{d\bar{y}^2} &= \frac{1}{2\bar{\lambda}^2}\left[\bar{n}_- - \bar{n}_+ + \bar{n}_{OH^-} - \bar{n}_{H^+}\right] \qquad [\text{for} \quad -1+\bar{d} \le \bar{y} \le 0] \\
&= \frac{1}{2\bar{\lambda}^2}\left[\left(1+\bar{n}_{H^+,\infty}\right)\exp\left(\bar{\psi}\right) - \exp\left(-\bar{\psi}\right) + \left(\bar{n}_{OH^-,\infty}\right)\exp\left(\bar{\psi}\right) - \left(\bar{n}_{H^+,\infty}\right)\exp\left(-\bar{\psi}\right)\right] \quad (3.10)
\end{aligned}$$

$$\begin{aligned}
\bar{\psi} &= -\frac{\ln\left(\frac{\bar{n}_{H^+}}{\bar{n}_{H^+,\infty}}\right)}{1+\frac{\bar{K}'_a\bar{\gamma}_a\varphi(\bar{y})}{\left(\bar{K}'_a+\bar{n}_{H^+}\right)^2}} \quad [\text{for} \quad -1 \le \bar{y} \le -1+\bar{d}], \\
\bar{\psi} &= -\ln\left(\frac{\bar{n}_{H^+}}{\bar{n}_{H^+,\infty}}\right) \qquad [\text{for} \quad -1+\bar{d} \le \bar{y} \le 0]. \qquad (3.11)
\end{aligned}$$

$$\begin{aligned}
\bar{\psi} &= \frac{\ln\left(\frac{\bar{n}_{OH^-}}{\bar{n}_{OH^-,\infty}}\right)}{1+\frac{\bar{K}'_b\bar{\gamma}_b\varphi(\bar{y})}{\left(\bar{K}'_b+\bar{n}_{OH^-}\right)^2}} \quad [\text{for} \quad -1 \le \bar{y} \le -1+\bar{d}], \\
\bar{\psi} &= \ln\left(\frac{\bar{n}_{OH^-}}{\bar{n}_{OH^-,\infty}}\right) \qquad [\text{for} \quad -1+\bar{d} \le \bar{y} \le 0]. \qquad (3.12)
\end{aligned}$$

The corresponding dimensionless boundary conditions obtained by non-dimensionalizing eq.(3.9) becomes:

$$\begin{aligned}
&\left(\frac{d\bar{\psi}}{d\bar{y}}\right)_{\bar{y}=0} = 0, \quad (\bar{\psi})_{\bar{y}=(-1+\bar{d})^+} = (\bar{\psi})_{\bar{y}=(-1+\bar{d})^-}, \quad \left(\frac{d\bar{\psi}}{d\bar{y}}\right)_{\bar{y}=(-1+\bar{d})^+} = \left(\frac{d\bar{\psi}}{d\bar{y}}\right)_{\bar{y}=(-1+\bar{d})^-}, \\
&\left(\frac{d\bar{\psi}}{d\bar{y}}\right)_{\bar{y}=-1} = 0. \qquad (3.13)
\end{aligned}$$

In the above equations, $\bar{y} = y/h$, $\bar{\lambda} = \lambda/h$ ($\lambda = \sqrt{\frac{\epsilon_0\epsilon_r k_B T}{2e^2\sum_i n_{i,\infty}}}$ is the EDL thickness), $\bar{d} = d/h$, $\bar{\psi} = e\psi/(k_B T)$, $\bar{n}_{H^+} = n_{H^+}/n_\infty$, $\bar{n}_{OH^-} = n_{OH^-}/n_\infty$, $\bar{n}_{H^+,\infty} = n_{H^+,\infty}/n_\infty$, $\bar{n}_{OH^-,\infty} = n_{OH^-,\infty}/n_\infty$, $\bar{K}'_a = K'_a/n_\infty$, and $\bar{\gamma}_a = \gamma_a/n_\infty$. Here $n_{+,\infty} = n_{-,\infty} = n_\infty =$

$10^3 N_A c_\infty$(c_∞ is the concentration in M, while n_∞ is the number density in $1/m^3$). Also as established in our previous studies [16,18], we can consider a cubic profile for $\varphi(y)$, i.e.,

$$\varphi(\bar{y}) = \beta\left(\bar{y}+1-\bar{d}\right)^2\left(\bar{y}+1+\frac{\bar{d}}{2}\right), \tag{3.14}$$

where $\beta = 4/\bar{d}^3$. We provide a detailed discussion later on this choice of the cubic profile later in the Discussion section.

Furthermore, as we are considering the PZI brush layer dissociation in an acidic solution, the concentration of the OH^- ions would be very small, so that we have $\bar{K}'_b \gg \bar{n}_{OH^-}$, and consequently eq.(3.12) reduces to:

$$\begin{aligned}
\bar{n}_{OH^-} &= \left(\bar{n}_{OH^-,\infty}\right)\exp\left[\bar{\psi}\left(1+\varphi\frac{\bar{\gamma}_b}{\bar{K}'_b}\right)\right] \qquad [\text{for} \quad -1 \le \bar{y} \le -1+\bar{d}],\\
\bar{n}_{OH^-} &= \left(\bar{n}_{OH^-,\infty}\right)\exp\left(\bar{\psi}\right) \qquad [\text{for} \quad -1+\bar{d} \le y \le 0].
\end{aligned} \tag{3.15}$$

Therefore, eq.(3.10) can be simplified as:

$$\begin{aligned}
&\frac{d^2\bar{\psi}}{d\bar{y}^2} = \frac{1}{2\bar{\lambda}^2}[(1+\bar{n}_{H^+,\infty})\exp(\bar{\psi}) - \exp(-\bar{\psi}) + (\bar{n}_{OH^-,\infty})\exp\left[\bar{\psi}(1+\varphi\frac{\bar{\gamma}_b}{\bar{K}'_b})\right] -\\
&\bar{n}_{H^+} + \varphi\frac{\bar{K}'_a\bar{\gamma}_a}{\bar{K}'_a+\bar{n}_{H^+}} - \varphi\bar{\gamma}_b] \qquad [\text{for} \quad -1 \le \bar{y} \le -1+\bar{d}],\\
&\frac{d^2\bar{\psi}}{d\bar{y}^2} = \frac{1}{2\bar{\lambda}^2}[(1+\bar{n}_{H^+,\infty})\exp(\bar{\psi}) - \exp(-\bar{\psi}) + (\bar{n}_{OH^-,\infty})\exp(\bar{\psi}) - (\bar{n}_{H^+,\infty})\exp(-\bar{\psi})]\\
&[\text{for} \quad -1+\bar{d} \le \bar{y} \le 0].
\end{aligned} \tag{3.16}$$

The explicit equilibrium electrostatic potential, H^+ and OH^- ion concentration distributions can be obtained by numerically solving the coupled equations [eqs.(3.11,3.15,3.16)]

in presence of the boundary condition expressed in (3.13).

Polyzwitterionic brush layer in basic solution

We next consider the case where the PZI brush layer is dissociating in a basic solution. We consider that the base furnishes the same cation as the salt. As a consequence, the bulk number density of the salt cation will be $n_\infty + n_{OH^-,\infty}$. Furthermore, the solution being basic, we would have $\bar{K}'_a \gg \bar{n}_{H^+}$, and consequently eq.(3.11) reduces to:

$$\begin{aligned}
\bar{n}_{H^+} &= \left(\bar{n}_{H^+,\infty}\right) \exp\left[-\bar{\psi}\left(1+\varphi\frac{\bar{\gamma}_a}{\bar{K}'_a}\right)\right] \qquad [\text{for} \quad -1 \le \bar{y} \le -1+\bar{d}], \\
\bar{n}_{H^+} &= \left(\bar{n}_{H^+,\infty}\right) \exp\left(-\bar{\psi}\right) \qquad [\text{for} \quad -1+\bar{d} \le y \le 0]. \quad (3.17)
\end{aligned}$$

Under these conditions, eq.(3.10) can be simplified as:

$$\begin{aligned}
&\frac{d^2\bar{\psi}}{d\bar{y}^2} = \frac{1}{2\bar{\lambda}^2}[\exp(\bar{\psi}) - (1+\bar{n}_{OH^-,\infty})\exp(-\bar{\psi}) + \bar{n}_{OH^-} - (\bar{n}_{H^+,\infty})\exp\left[-\bar{\psi}(1+\varphi\frac{\bar{\gamma}_a}{\bar{K}'_a})\right] + \varphi\bar{\gamma}_a \\
&- \varphi\frac{\bar{K}'_b\bar{\gamma}_b}{\bar{K}'_b+\bar{n}_{OH^-}}] \quad [\text{for} \ -1 \le \bar{y} \le -1+\bar{d}], \\
&\frac{d^2\bar{\psi}}{d\bar{y}^2} = \frac{1}{2\bar{\lambda}^2}[\exp(\bar{\psi}) - (1+\bar{n}_{OH^-,\infty})\exp(-\bar{\psi}) + (\bar{n}_{OH^-,\infty})\exp(\bar{\psi}) - (\bar{n}_{H^+,\infty})\exp(-\bar{\psi})] \\
&[\text{for} \ -1+\bar{d} \le \bar{y} \le 0]. \qquad (3.18)
\end{aligned}$$

The explicit equilibrium electrostatic potential, H^+ and OH^- ion concentration distributions can be obtained by numerically solving the coupled equations [eqs.(3.12,3.17,3.18)] in presence of the boundary condition expressed in (3.13).

3.2.2 Velocity Field

The pressure-driven transport considered here would give rise to an electric field. This electric field will drive an electroosmotic (EOS) flow, whose direction would always be opposite to the direction of the pressure-driven transport. Considering this overall velocity field (which is a combination of the pressure-driven transport and an EOS flow) to be steady, uni-directional and hydrodynamically fully-developed, we can express it for the channel bottom half as:

$$\eta\frac{d^2u}{dy^2} - \frac{dp}{dx} + eE_S(n_+ - n_- + n_{H^+} - n_{OH^-}) - \frac{\eta}{\kappa}u = 0 \qquad [-h \le y \le -h+d]\,,$$
$$\eta\frac{d^2u}{dy^2} - \frac{dp}{dx} + eE_S(n_+ - n_- + n_{H^+} - n_{OH^-}) = 0 \qquad [-h+d \le y \le 0]\,. \qquad (3.19)$$

In eq.(3.19), $-dp/dx$ is the employed pressure gradient, η is the dynamic viscosity of the liquid, e is the electronic charge, n_i is the number density of the ionic species i, and $\kappa = a_k^2\left(\frac{d}{\sigma a_k^3 N_p \varphi}\right)^2$ is the permeability and $\frac{\sigma a_k^3 N_p \varphi}{d}$ is the volume fraction of the PZI brush layer. For the present study, we consider the cubic profile for φ [see eq(3.14)]. Of course, the solution of the velocity field u would be sought in presence of the known distribution of ψ, $n_\pm$, n_{H^+}, and n_{OH^-}.

Using the calculations provided in the previous section, eq.(3.19) can be expressed in dimensionless form as:

In acidic solution:

$$0 = \frac{d^2\bar{u}}{d\bar{y}^2} - 1 + \frac{\bar{E}_S}{2\bar{\lambda}^2}[\exp(-\bar{\psi}) - (1+\bar{n}_{H^+,\infty})\exp(\bar{\psi}) + \bar{n}_{H^+} - \bar{n}_{OH^-,\infty}\exp[\bar{\psi}(1+\varphi\frac{\bar{\gamma}_b}{\bar{K}_b'})]]$$

$$-\bar{\alpha}^2\phi^2\bar{u} \qquad [-1 \le \bar{y} \le -1+\bar{d}],$$

$$0 = \frac{d^2\bar{u}}{d\bar{y}^2} - 1 + \frac{\bar{E}_S}{2\bar{\lambda}^2}[\exp(-\bar{\psi}) - (1+\bar{n}_{H^+,\infty})\exp(\bar{\psi}) + \bar{n}_{H^+,\infty}\exp(-\bar{\psi}) - \bar{n}_{OH^-,\infty}\exp(\bar{\psi})]$$

$$[-1+\bar{d} \le \bar{y} \le 0]. \tag{3.20}$$

In basic solution:

$$0 = \frac{d^2\bar{u}}{d\bar{y}^2} - 1 + \frac{\bar{E}_S}{2\bar{\lambda}^2}[(1+\bar{n}_{OH^-,\infty})\exp(-\bar{\psi}) - \exp(\bar{\psi}) + \bar{n}_{H^+,\infty}\exp[-\bar{\psi}(1+\varphi\frac{\bar{\gamma}_a}{\bar{K}_a'})] - \bar{n}_{OH^-}]$$

$$-\bar{\alpha}^2\phi^2\bar{u} \qquad [-1 \le \bar{y} \le -1+\bar{d}],$$

$$0 = \frac{d^2\bar{u}}{d\bar{y}^2} - 1 + \frac{\bar{E}_S}{2\bar{\lambda}^2}[(1+\bar{n}_{OH^-,\infty})\exp(-\bar{\psi}) - \exp(\bar{\psi}) + \bar{n}_{H^+,\infty}\exp(-\bar{\psi}) - \bar{n}_{OH^-,\infty}\exp(\bar{\psi})]$$

$$[-1+\bar{d} \le \bar{y} \le 0]. \tag{3.21}$$

In eqs. (3.20, 3.21), $\bar{u} = \frac{u}{u_{p,0}}$ (where $u_{p,0} = \frac{h^2}{\eta}\frac{dp}{dx}$ is pressure-driven velocity scale), $\bar{E}_S = \frac{E_S}{E_0}$ (where $E_0 = \frac{e\eta u_{p,0}}{\epsilon_0\epsilon_r k_B T} = \frac{dp}{dx}\frac{eh^2}{\epsilon_0\epsilon_r k_B T}$ is the scale of the electric field), and $\bar{\alpha} = \frac{\sigma a_k^2 N_p}{\bar{d}}$. $u_r = \frac{u_{e,0}}{u_{p,0}}$ is taken to be unity where $u_{e,0} = \frac{k_B T}{e}\frac{\epsilon_0\epsilon_r E_0}{\eta}$ is the electroosmotic velocity scale. Solution of eqs.(3.20, 3.21) are sought in presence of the following dimensionless boundary conditions:

$$(\bar{u})_{\bar{y}=-1} = 0; \quad \left(\frac{d\bar{u}}{d\bar{y}}\right)_{\bar{y}=0} = 0; \quad (\bar{u})_{\bar{y}=(-1+\bar{d})^+} = (\bar{u})_{\bar{y}=(-1+\bar{d})^-};$$
$$\left(\frac{d\bar{u}}{d\bar{y}}\right)_{\bar{y}=(-1+\bar{d})^+} = \left(\frac{d\bar{u}}{d\bar{y}}\right)_{\bar{y}=(-1+\bar{d})^-}. \tag{3.22}$$

Of course, the solution of $\bar{u}$ requires the value of the $\bar{E}_S$. Calculation of $\bar{E}_S$ is discussed in the following subsection.

3.2.3 Streaming electric field E_S

To obtain E_S, we consider that the net ionic current (per unit width) i is equal to zero, i.e.,

$$i = 2e \int_{-h}^{0} (u_+ n_+ - u_- n_- + u_{H^+} n_{H^+} - u_{OH^-} n_{OH^-})\, dy = 0, \tag{3.23}$$

where u_i $(i = \pm, H^+, OH^-)$ is the ion migration velocity, expressed as:

$$u_i = u + \frac{e z_i E_S}{f_i}. \tag{3.24}$$

Here f_i is the ionic friction coefficient and z_i is the valence for ion i. Substituting eq.(3.24) in eq.(3.23), we finally obtain the dimensionless streaming electric field as:

In acidic solution:

$$\bar{E}_S = \frac{\int_{-1}^{0} \bar{u} \left[-\exp(-\bar{\psi}) + (1 + \bar{n}_{H^+,\infty}) \exp(\bar{\psi}) - \bar{n}_{H^+} + \bar{n}_{OH^-} \right] d\bar{y}}{\int_{-1}^{0} [R_+ \exp(-\bar{\psi}) + R_- (1 + \bar{n}_{H^+,\infty}) \exp(\bar{\psi}) + R_{H^+} \bar{n}_{H^+} + R_{OH^-} \bar{n}_{OH^-})] d\bar{y}}. \tag{3.25}$$

In basic solution:

$$\bar{E}_S = \frac{\int_{-1}^{0} \bar{u} \left[-(1 + \bar{n}_{OH^-,\infty}) \exp(-\bar{\psi}) + \exp(\bar{\psi}) - \bar{n}_{H^+} + \bar{n}_{OH^-} \right] d\bar{y}}{\int_{-1}^{0} [R_+ (1 + \bar{n}_{OH^-,\infty}) \exp(-\bar{\psi}) + R_- \exp(\bar{\psi}) + R_{H^+} \bar{n}_{H^+} + R_{OH^-} \bar{n}_{OH^-})] d\bar{y}}. \tag{3.26}$$

where $R_i = \frac{e^2 z_i^2 \eta}{\epsilon_0 \epsilon_r k_B T f_i}$ is a dimensionless parameter, often interpreted as the inverse of the ionic Peclet number. We take $f = \frac{eE_0}{u_{p,0}} = \frac{e^2 \eta}{\epsilon_0 \epsilon_r k_B T}$. Of course, we would use eq.(3.25) in eq.(3.20) to obtain the integro-differential equation governing the velocity field $\bar{u}$ within the PZI-brush-grafted nanochannel in acidic condition; on the other hand, we would use eq.(3.26) in eq.(3.21) to obtain the integro-differential equation governing the velocity field $\bar{u}$ within the PZI-brush-grafted nanochannel in basic condition. The integro-differential equations for both the cases are solved numerically in presence of the BCs expressed in eq.(3.22). We were the first group to develop and solve such highly involved integro-differential equations for obtaining the streaming electric field and the resulting electrokinetics in nanochannels grafted with charged polyelectrolyte brushes [19, 84, 111] – in this study, we again use that theoretical framework to compute the induced electrokinetics in nanochannels grafted with the PZI brushes.

3.2.4 Efficiency of the electrochemomechanical energy conversion

Generation of the nanofluidic streaming current (i_S) and the streaming electric field (E_S) is a process of nanoscale electrochemomechanical energy conversion, since the mechanical energy of the pressure-driven flow and the chemical energy of the EDL are converted to the electrical energy associated with the generation of i_S and E_S. This efficiency ξ of this energy conversion can be expressed as:

$$\xi = \frac{P_{out}}{P_{in}}. \tag{3.27}$$

Here P_{in} and P_{out} are the input and the output powers (per unit area), expressed as:

$$P_{out} = \frac{1}{4} i_S E_S, \quad P_{in} = \left| -\frac{dp}{dx} \right| Q_{in}. \tag{3.28}$$

Here the streaming current is

$$i_S = 2e \int_{-h}^{0} u \left(n_+ - n_- + n_{H^+} - n_{OH^-} \right) dy, \tag{3.29}$$

or in a dimensionless form:

$$\bar{i}_S = \int_{-1}^{0} \bar{u} \left(\bar{n}_+ - \bar{n}_- + \bar{n}_{H^+} - \bar{n}_{OH^-} \right) d\bar{y}, \tag{3.30}$$

where $\bar{i}_S = \frac{i_s}{2hen_\infty u_{p,0}}$ and Q_{in} is the the input volume flow rate per unit width, expressed as:

$$Q_{in} = 2 \int_{-h}^{0} u_p dy. \tag{3.31}$$

Here u_p is the pure pressure-driven velocity field governed by the following equations:

$$\begin{aligned} \eta \frac{d^2 u_p}{dy^2} - \frac{dp}{dx} - \frac{\eta}{\kappa} u_p = 0, \qquad & \left[-h \le y \le -h + d_0 \right], \\ \eta \frac{d^2 u_p}{dy^2} - \frac{dp}{dx} = 0, \qquad & \left[-h + d_0 \le y \le 0 \right]. \end{aligned} \tag{3.32}$$

For the acidic solution, we can therefore obtain [using eqs.(3.25,3.27,3.28,3.30,3.31)]:

$$\xi = \frac{1}{8\bar{\lambda}^2 \int_{-1}^{0} \bar{u}_p d\bar{y}} \frac{\left[\int_{-1}^{0} \bar{u} \left[-\exp(-\bar{\psi}) + (1 + \bar{n}_{H^+,\infty}) \exp(\bar{\psi}) - \bar{n}_{H^+} + \bar{n}_{OH^-} \right] d\bar{y} \right]^2}{\int_{-1}^{0} [\exp(-\bar{\psi}) + (1 + \bar{n}_{H^+,\infty}) \exp(\bar{\psi}) + \bar{n}_{H^+} + \bar{n}_{OH^-}] d\bar{y}}. \tag{3.33}$$

On the other hand, for the basic solution we can obtain [using eqs.(3.26,3.27,3.28,3.30,3.31)]:

In Basic Solution:

$$\xi = \frac{1}{8\bar{\lambda}^2 \int_{-1}^{0} \bar{u}_p d\bar{y}} \frac{\left[\int_{-1}^{0} \bar{u} \left[-(1 + \bar{n}_{OH^-,\infty}) \exp(-\bar{\psi}) + \exp(\bar{\psi}) - \bar{n}_{H^+} + \bar{n}_{OH^-} \right] d\bar{y} \right]^2}{\int_{-1}^{0} [\exp(-(1 + \bar{n}_{OH^-,\infty})\bar{\psi}) + \exp(\bar{\psi}) + \bar{n}_{H^+} + \bar{n}_{OH^-}] d\bar{y}}. \tag{3.34}$$

Of course, both eqs.(3.33,3.34) can be simplified to a unique form expressed as:

$$\xi = \frac{1}{8\bar{\lambda}^2 \int_{-1}^{0} \bar{u}_p d\bar{y}} \frac{\bar{i}_S^2}{\bar{i}_C} = \frac{\bar{i}_C \bar{E}_S^2}{8\bar{\lambda}^2 \int_{-1}^{0} \bar{u}_p d\bar{y}}. \tag{3.35}$$

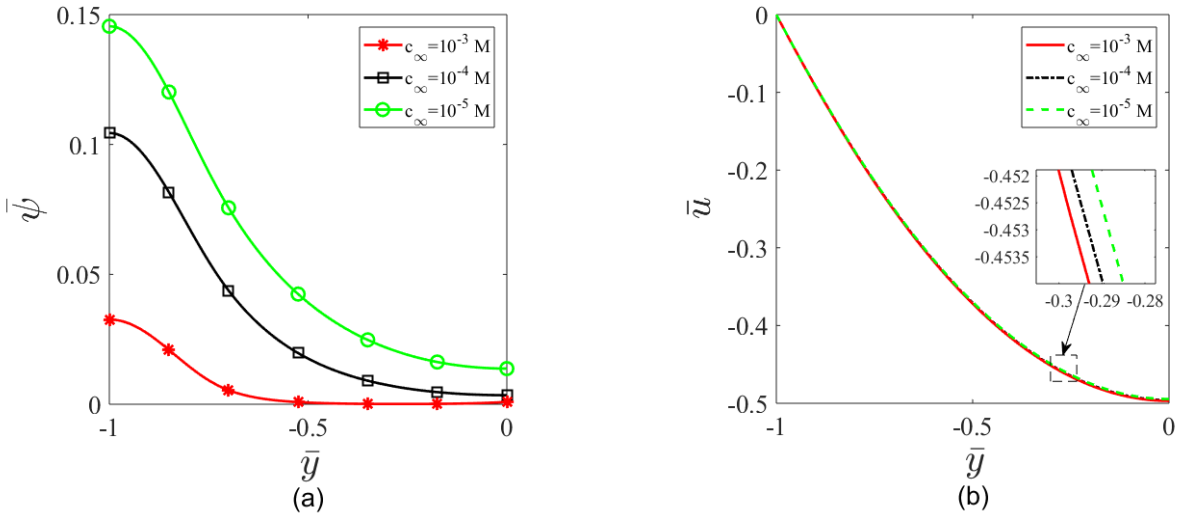

Figure 3.2: *Transverse variation of (a) dimensionless electrostatic potential* $\bar{\psi}$ *and (b) dimensionless velocity profile* $\bar{u}$ *for different values of bulk salt concentration* c_∞. *Other parameters for this figure are* $pH_\infty = 4$ *(or bulk pH),* $pK_a = 4$, $pK_b = 4$, $\bar{d} = 0.3$, $\gamma_a = 10^{-4}M$, $\gamma_b = 10^{-4}M$, $\bar{\alpha} = 1$, $u_r = 1$, $R_i = 1$, $\frac{N_p a^3 \sigma}{d} = 1$, $h = 100nm$, $k_B = 1.38 \times 10^{-23}J/K$, $T = 300K$, $e = 1.6 \times 10^{-19}C$, $\epsilon_0 = 8.854 \times 10^{-12}F/m$, $\epsilon_r = 79.8$.

3.3 Results

In Figures 3.2-3.9, we provide the transverse variation of the dimensionless electrostatic potential ($\bar{\psi}$) and the dimensionless velocity ($\bar{u}$) for different combinations of the system parameters. An acidic solution (characterized by $pH_\infty < 7$) implies

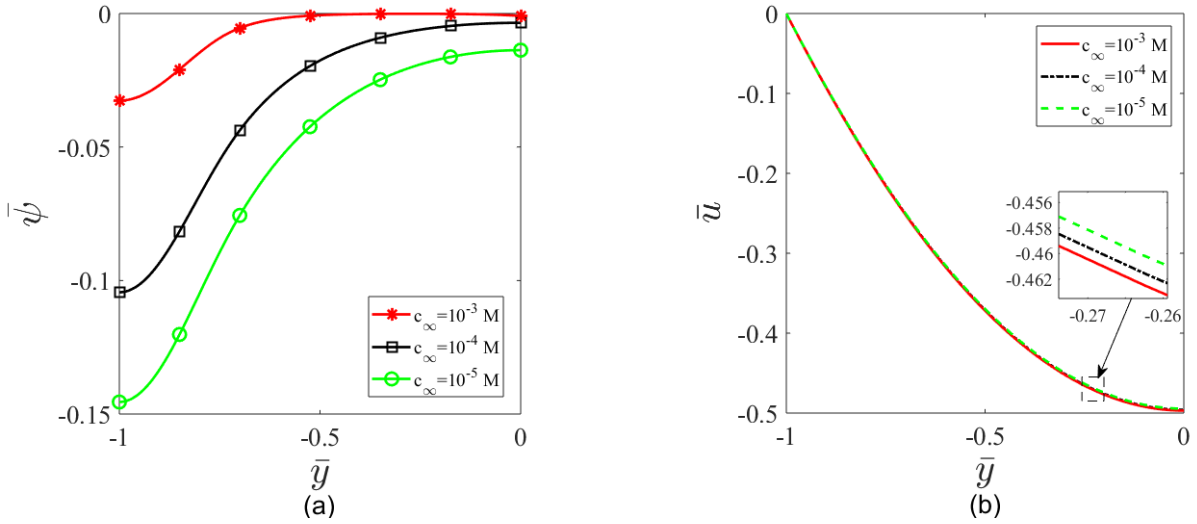

Figure 3.3: *Transverse variation of (a) $\bar{\psi}$ and (b) $\bar{u}$ for different values of c_∞. Here we consider $pH_\infty = 10$ (bulk pH). All other parameters are identical to that used in figure 3.2.*

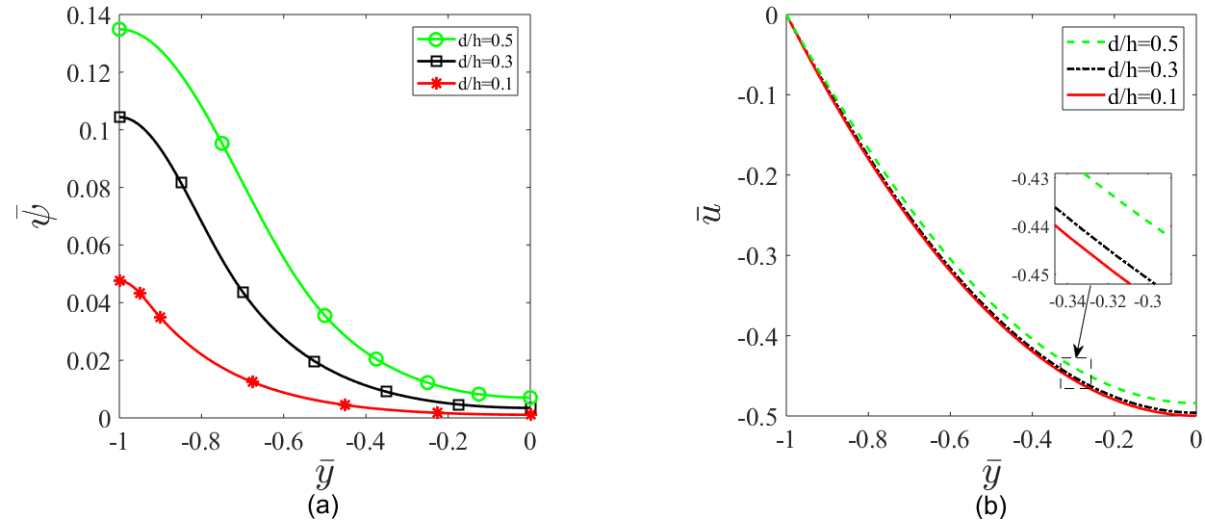

Figure 3.4: *Transverse variation of (a) $\bar{\psi}$ and (b) $\bar{u}$ for different values of $\bar{d}$. Here we consider $c_\infty = 10^{-4}M$. All other parameters are identical to that used in figure 3.2.*

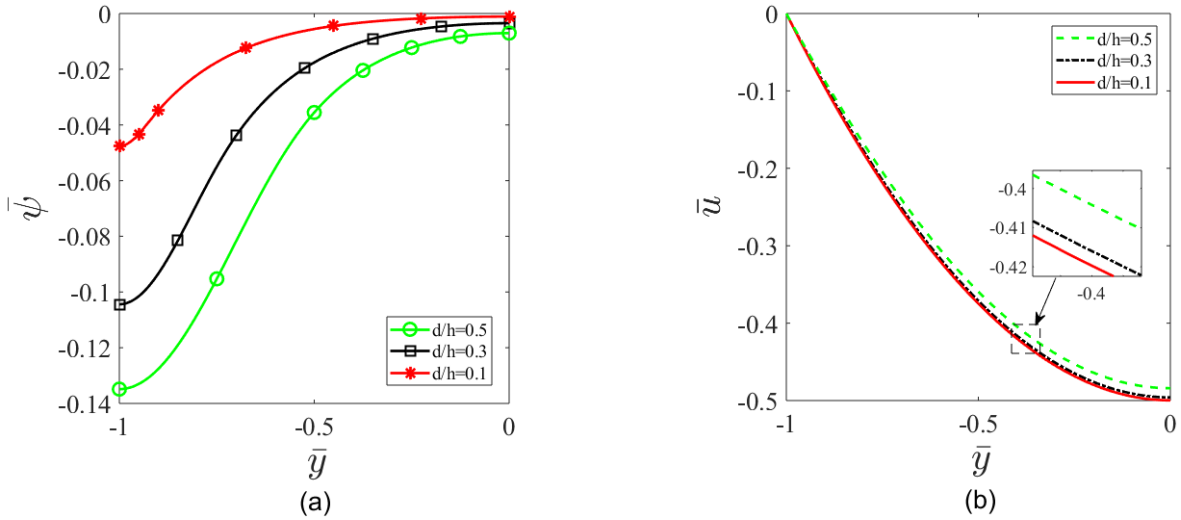

Figure 3.5: *Transverse variation of (a) $\bar{\psi}$ and (b) $\bar{u}$ for different values of $\bar{d}$. Here we consider $c_\infty = 10^{-4}M$. All other parameters are identical to that used in figure 3.3.*

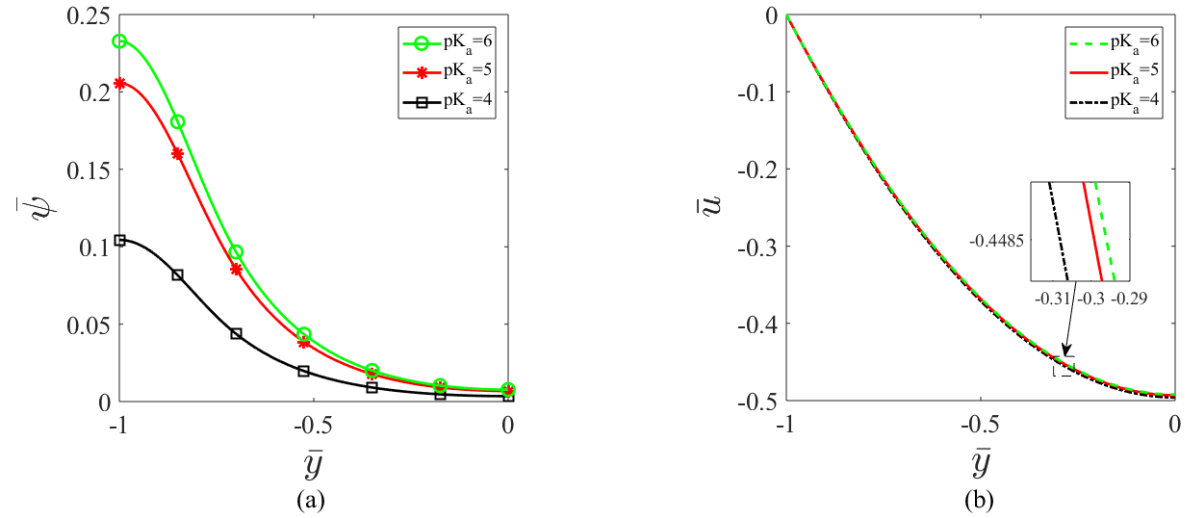

Figure 3.6: *Transverse variation of (a) $\bar{\psi}$ and (b) $\bar{u}$ for different values of pK_a. Here we consider $c_\infty = 10^{-4}M$. All other parameters are identical to that used in figure 3.2.*

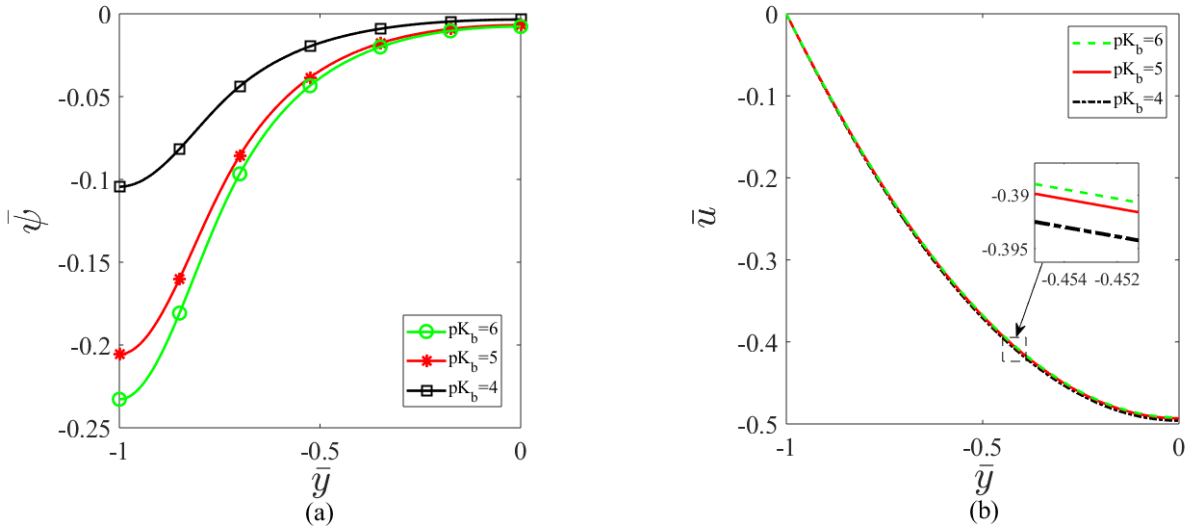

Figure 3.7: *Transverse variation of (a) $\bar{\psi}$ and (b) $\bar{u}$ for different values of pK_a. Here we consider $c_\infty = 10^{-4}M$. All other parameters are identical to that used in figure 3.3.*

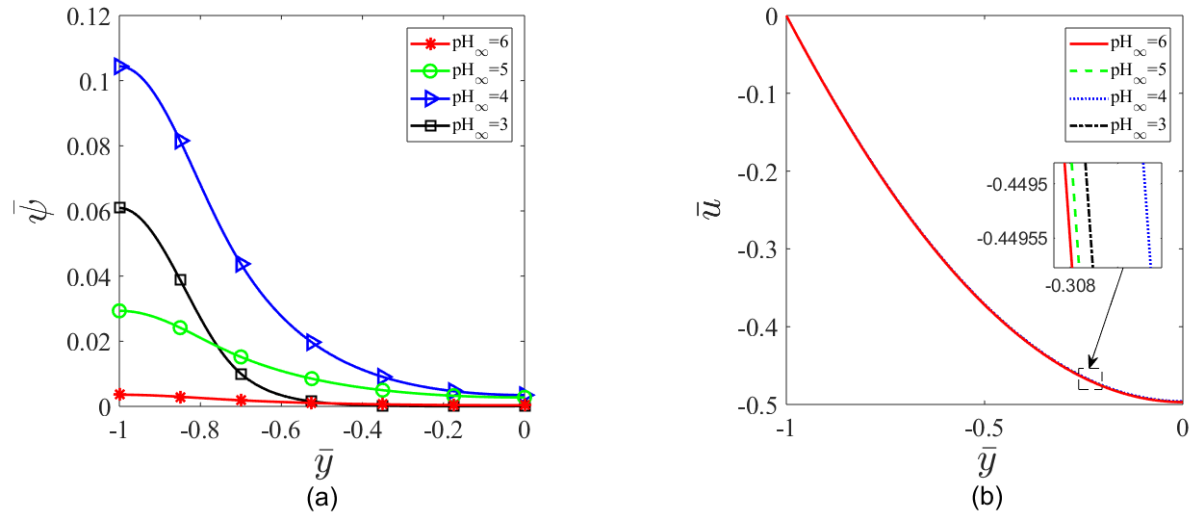

Figure 3.8: *Transverse variation of (a) $\bar{\psi}$ and (b) $\bar{u}$ for different pH_∞ (bulk pH) values in an acidic solution. Here we consider $c_\infty = 10^{-4}M$. All other parameters are identical to that used in figure 3.2.*

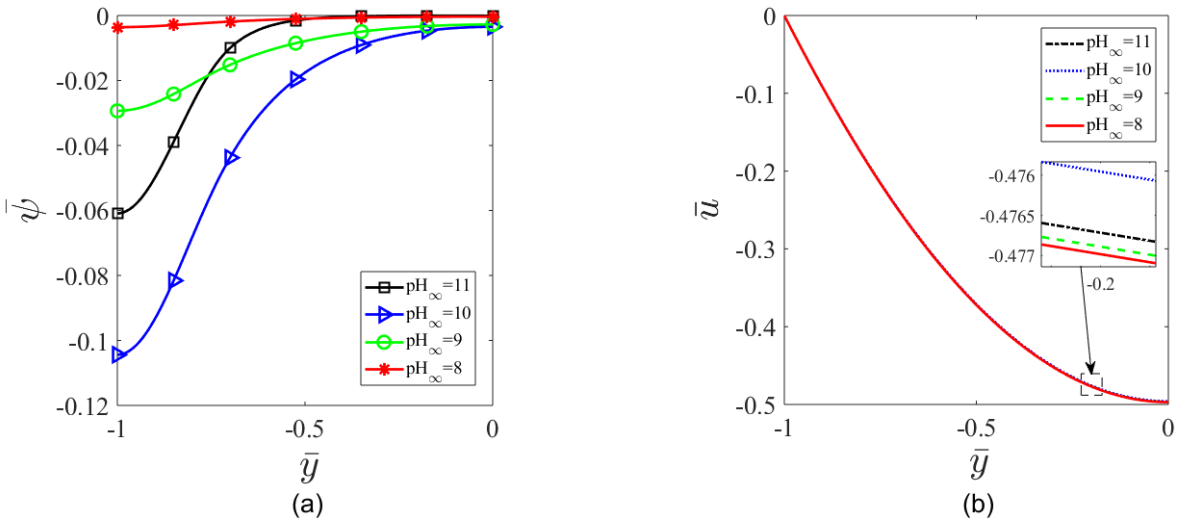

Figure 3.9: *Transverse variation of (a) $\bar{\psi}$ and (b) $\bar{u}$ for different pH_∞ (bulk pH) values in a basic solution. Here we consider $c_\infty = 10^{-4}M$. All other parameters are identical to that used in figure 3.2.*

the presence of more H^+ ions than OH^- ions. As a consequence, the ionization that produces the BH^+ charged group (this ionization produces more OH^- ions) is more preferred than the ionization that produces the A^- group (this ionization produces more H^+ ions). Therefore, for such a pH (< 7), the PZI attains a net positive charge under identical values of pK_a and pK_b leading to a positive value of the corresponding $\bar{\psi}$. This is evident in Figures 3.2(a), 3.4(a), 3.6(a), and 3.8(a). On the other hand, a basic solution (characterized by $pH_\infty > 7$) has more OH^- ions than H^+ ions. Accordingly the ionization that produces H^+ ions (i.e., the ionization that produces the A^- group of the PZI) is much more preferred than the ionization that produces the OH^- ions (i.e., the ionization that produces the BH^+ group of the PZI). As a consequence, for such a pH_∞ (> 7), the PZI attains a net negative charge under identical

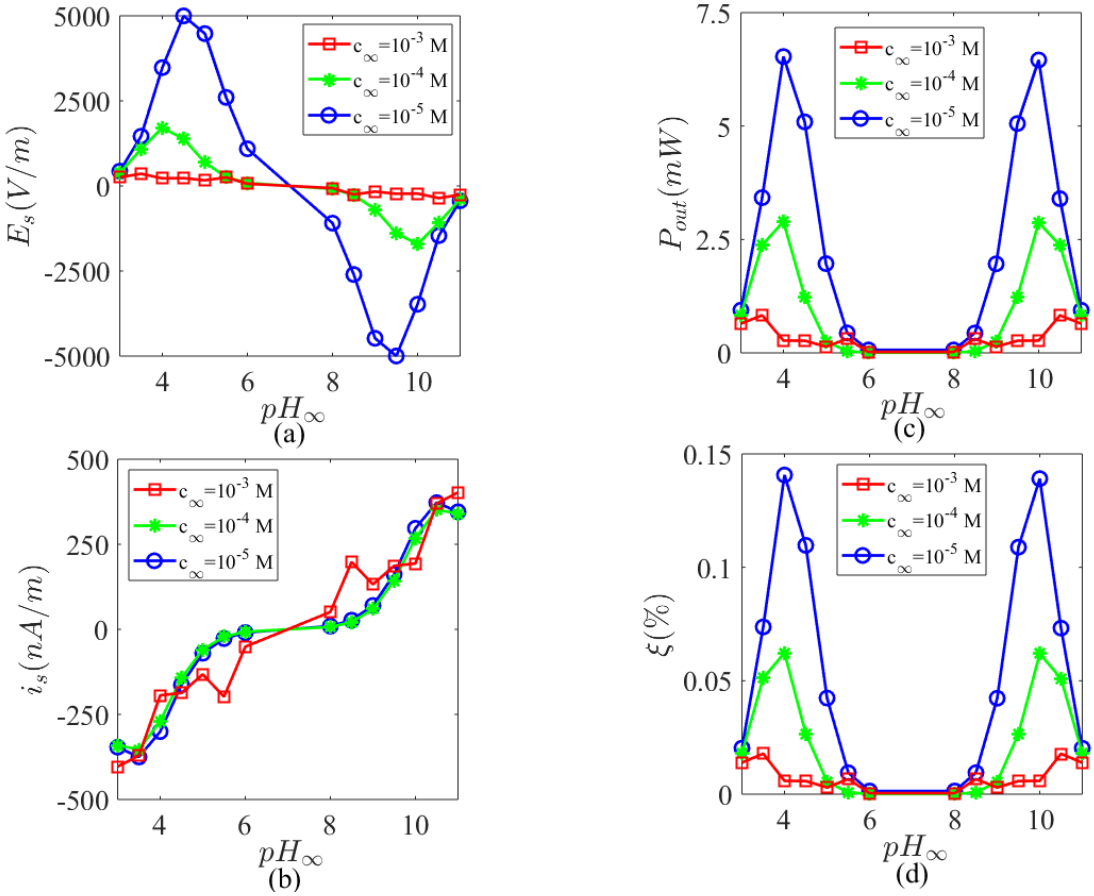

Figure 3.10: *Variation of (a) streaming electric field E_s, (b) steaming current i_s, (c) output power P_{out} and (d) electrochemomechanical energy conversion efficiency ξ with pH_∞ for different values of c_∞. In order to calculate the power, we use $\frac{dp}{dx} = -5 \times 10^8 Pa/m$, $\eta = 8.9 \times 10^{-4} Pa \cdot s$, and consider a nanofluidic chip that is $1mm \times 10cm \times 10cm$ in dimensions (i.e., 1 mm in length and 10 cm in both breadth and width) with a porosity of 0.5. All other parameters are identical to that used in figure 3.2.*

values of pK_a and pK_b leading to a negative value of the corresponding $\bar{\psi}$ [see Figures 3.3(a), 3.5(a), 3.7(a), and 3.9(a)]. For both the cases of positive and negative $\bar{\psi}$, a

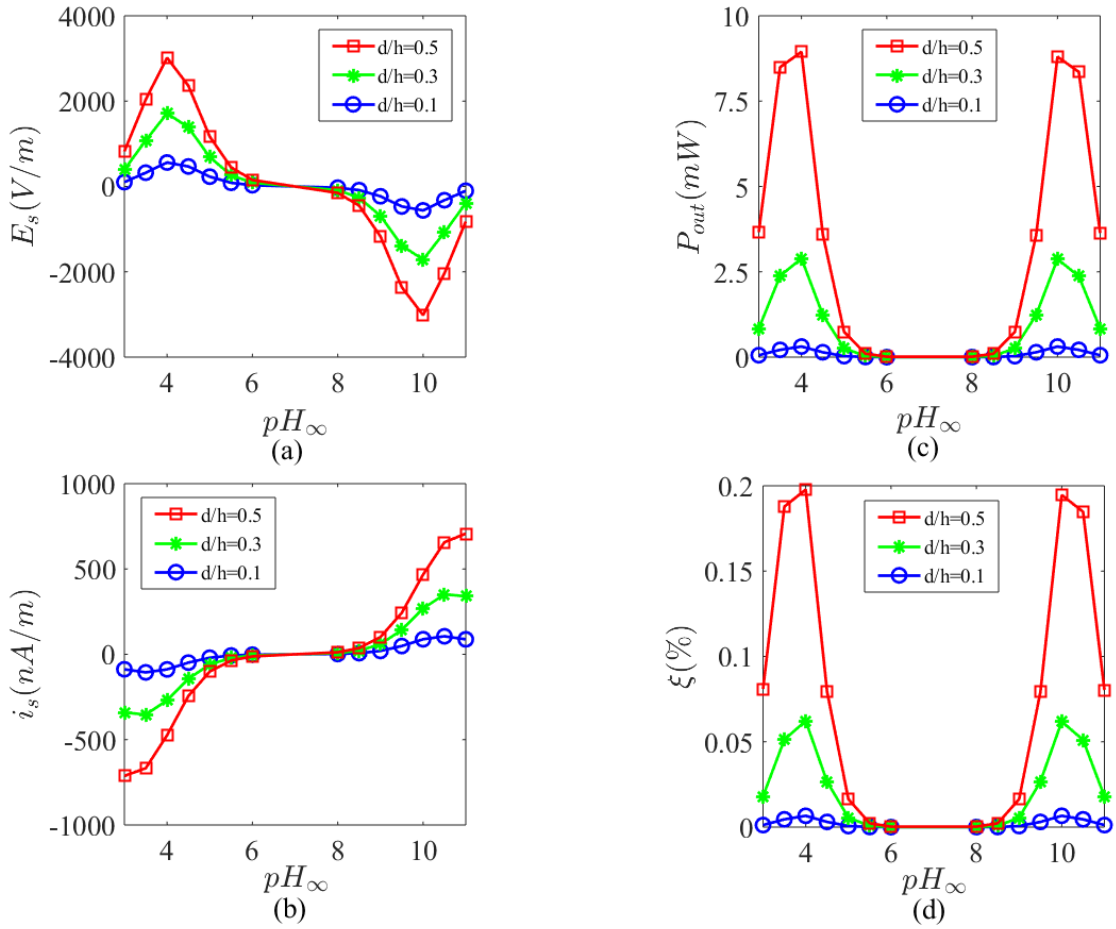

Figure 3.11: *Variation of (a) E_s, (b) i_s, (c) P_{out} and (d) ξ with pH_∞ for different values of $\bar{d}$. Here we use $c_\infty = 10^{-4}$ M. All other parameters are identical to that used in figure 3.10.*

decrease in the salt concentration (c_∞) increases the magnitude of $\bar{\psi}$. Smaller c_∞ leads to a larger EDL thickness (λ), which would imply a larger $\bar{\psi}$ for a given charge density (σ), attributed to the fact that $d\psi/dy \sim \sigma/(\epsilon_0\epsilon_r) \Rightarrow \psi \sim \sigma\lambda/(\epsilon_0\epsilon_r)$. This is evident In Figures 3.2(a) and 3.3(a). Furthermore, an increase in the relative brush height (or larger d/h value) leads to a larger charge content of the system leading to a greater magnitude (either positive or negative) of $\bar{\psi}$ [see Figures 3.4(a) and 3.5(a)].

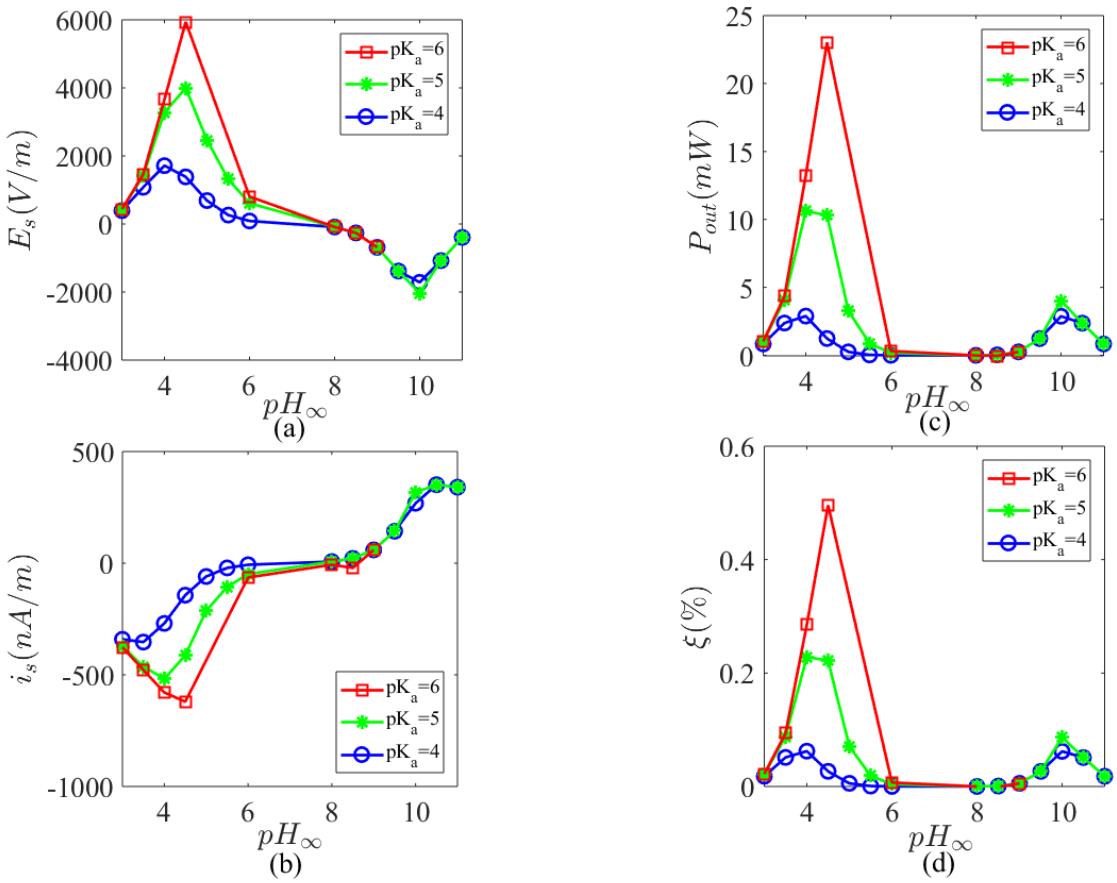

Figure 3.12: *Variation of (a) E_s, (b) i_s, (c) P_{out} and (d) ξ with pH_∞ for different values of pK_a. Here we use $c_\infty = 10^{-4}$ M. All other parameters are identical to that used in figure 3.10.*

A larger value of pK_a for the case where the charging of the PZI is dominated by the formation of the positive sites (i.e., the situation that occurs at an acidic pH or $pH_\infty < 7$) implies that the ionization of the PZI to produce the negative sites is retarded and therefore leads to a large net positive charge on the PZI and a larger positive magnitude of $\bar{\psi}$. This is depicted in Figure 3.6(a). Exactly reverse occurs for a basic solution ($pH > 7$) and larger pK_b. For such a solution, the PZI charge is

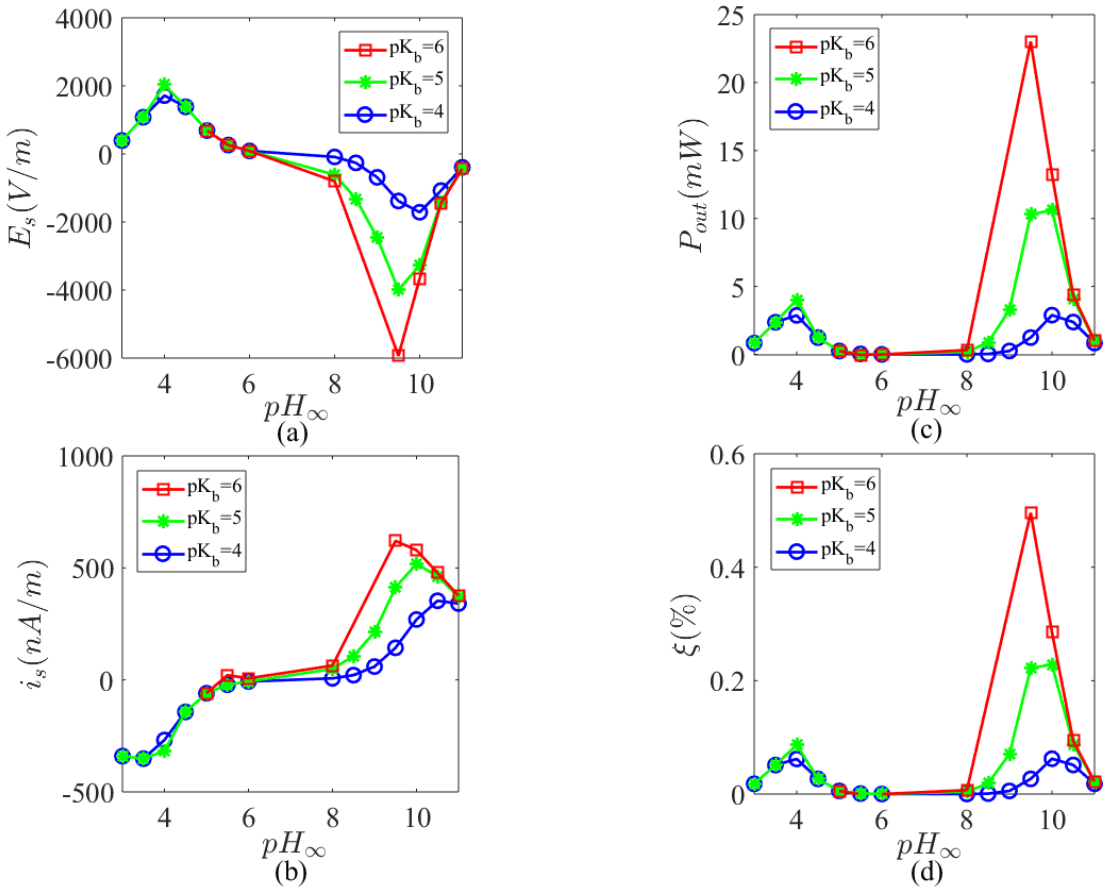

Figure 3.13: *Variation of (a) E_s, (b) i_s, (c) P_{out} and (d) ξ with pH_∞ for different values of pK_b. Here we use $c_\infty = 10^{-4}$ M. All other parameters are identical to that used in figure 3.10.*

dominated by the formation of the negative sites and a larger pK_b implies a weaker ionization of the positive sites making the PZI more negative (and hence $\bar{\psi}$ more negative). This is depicted in Figure 3.7(a). Finally in Figures 3.8 and 3.9, we show the effect of the variation in pH_∞. In the acidic range, a progressive lowering of pH_∞ (or a progressive increase in the the number of H^+ ions) implies a more retarded ionization of the negative group of the PZI (this ionization produced H^+ ions) implying a

larger manifestation of the positive charge of the PZI ensuring a larger positive value of $\bar{\psi}$. This is witnessed for pH_∞ values varying from 6 to 4. However, for $pH_\infty = 3$, we find that the $\bar{\psi}$ becomes smaller than that at $pH_\infty = 4$. The reason is that since we operate at $c_\infty = 10^{-4}\ M$, at $pH = 3$ (or $c_{H^+,\infty} = 10^{-3}\ M$), the hydrogen ion concentration dictates the EDL thickness causing a decrease in the EDL thickness as compared to the case when $pH_\infty = 4$. This lowering of the EDL thickness reduces the overall $\bar{\psi}$. This behavior is witnessed in Figure 3.8(a). On the other hand, in the basic range, a progressive increase in pH_∞ implying a progressive lowering of pOH_∞ (or a progressive increase in the number of OH^- ions), leads to a suppression of the ionization that generates positive charge of the PZI (this ionization also produces the OH^- ion) enforcing a larger negative charge of the PZI. Therefore, one witnesses a progressively larger negative magnitude of $\bar{\psi}$ as pH_∞ increases from 8 to 10. However, at $pH_\infty = 11$ or $pOH_\infty = 3$, the concentration of the OH^- ions dictates the EDL thickness making the EDL thickness smaller than that for $pH_\infty = 10$ (or $pOH_\infty = 4$) enforcing a reduction in $\bar{\psi}$ [see Figure 3.9(a)].

The part (b) of Figs. 3.2-3.9 provide the variation of the overall velocity field for the different combination of the system parameters. The overall velocity field is a combination of the pressure-driven transport (caused by the employed pressure gradient) and the induced EOS transport caused by the induced streaming electric field [shown in Figures 3.10-3.13(a)]. Regardless of the value of pH_∞ (or the corresponding sign of the net charge on the PZI), the EOS transport always opposes the pressure-driven transport and hence reduces the overall transport. Please note that here both the pressure-driven transport and hence the overall transport are positive

– however, the net transport appears negative as we non-dimensionalize the velocity field by a characteristic velocity that is negative (i.e., $u_{p,0} = \frac{h^2}{\eta}\frac{dp}{dx} < 0$). The induced electric field (E_s) driving the EOS transport is positive for the acidic pH and negative for the basic pH [see Figs. 3.10-3.13(a)]. E_s is induced by the downstream migration of the non-zero charge density of the EDL. For the acidic pH, the PZI is positively charged (manifested by a positive magnitude of $\bar{\psi}$); therefore the counterions will be anions. Thus the downstream migration of the EDL charge density would imply a net downstream migration of the negative charges, thereby leading to a larger downstream accumulation of the negative charges. Therefore the net potential will be more positive on the upstream side than the downstream side, ensuring that the electric field is positive (i.e., from left to right). This electric field interacts with the net EDL charge density to induce the EOS transport. The per unit volume EOS body force is $f_{EOS} = e(n_+ - n_-)E_s$. Of course, a positive E_s occurs when $n_- > n_+$ (as already discussed above) ensuring $f_{EOS} < 0$ and hence $u_{EOS} < 0$. For a basic pH, the net PZI charge is negative making the counterions positive and therefore the downstream advection of the EDL charge density leads to a downstream accumulation of the positive ions. This ensures that the net potential is more positive downstream, enforcing $E_s < 0$. Of course, as $n_+ > n_-$ for this case, $f_{EOS} = e(n_+ - n_-)E_s < 0$ and $u_{EOS} < 0$ for this case as well.

A larger magnitude of $\bar{\psi}$ leads to a larger difference between the counterion and coion number density within an EDL, which in turn would enforce both a larger magnitude of E_s and an even larger magnitude of f_{EOS}. Therefore, cases with a larger magnitude of $\bar{\psi}$ would result in a larger magnitude of u_{EOS} and hence a larger

reduction in the overall velocity field. Therefore, we witness a lesser velocity for a weaker salt concentration [see Figures 3.2(b) and 3.3(b)], for a larger brush height [see Figures 3.4(b) and 3.5(b)], for a larger pK_a for acidic solution [see Fig. 3.6(b)], for a larger pK_b for basic solution [see Fig. 3.7(b)], for smaller pH_∞ for acidic solution [see Fig. 3.8(b)] (except for very small pH_∞ where the hydrogen ion number density dictates the EDL thickness), and for larger pH_∞ for basic solution [see Fig. 3.9(b)] (except for very large pH_∞ where the hydroxyl ion number density dictates the EDL thickness).

Figs. 3.10-3.13(a) provide the variation of the streaming electric field E_s with pH_∞ for different system parameters. We invariably find a positive (negative) E_s for acidic (basic) pH. As we have already discussed above, such a behavior can be attributed to the net positive (negative) charge of the PZI leading to anions (cations) becoming the counterions at an acidic (basic) pH. Also all the factors that lead to an enhancement in the magnitude of $\bar{\psi}$ [see Figures 3.2-3.9(a)] would augment the magnitude of E_s. Such a connection directly follows from the fact that a larger magnitude of $\bar{\psi}$ would imply a larger difference in the number densities between the counterions and coions, and hence a larger magnitude of the electrostatic potential difference (caused by the flow-driven downstream accumulation of the counterions) leading to a larger E_s. Therefore, one witnesses a larger magnitude of E_s for a weaker salt concentration [see Figure 3.10(a)], for a larger brush height [see Figure 3.11(a)], for a larger pK_a for an acidic solution [see Figure 3.12(a)], for a larger pK_b for a basic solution [see Figure 3.13(a)], for smaller pH_∞ for acidic solution [see Figures 3.10-3.13(a)] (except for very small pH_∞ where the hydrogen ion number density

dictates the EDL thickness and this ensures a maximum in the magnitude of E_s at an intermediate pH_∞), and for larger pH_∞ for basic solution [see Figures 3.10-3.13(a)] (except for very large pH_∞ where the hydroxyl ion number density dictates the EDL thickness and this ensures a minimum or a negative maximum in the magnitude of E_s at an intermediate pOH_∞). A critical observation from all the E_s plots is a remarkable symmetry (in magnitude) across the pH_∞ spectrum. In other words, we get the same magnitude (with different sign) for same values of pH_∞ and pOH_∞ (i.e., at large and small pH_∞). This obviously stems from the fact that PZI becomes charged at these extreme pH_∞ values. Therefore, this study points to this unique opportunity where one can attain a large magnitude of E_s for both large and small pH.

Figures 3.10-3.13(b) provides the variation of the streaming current i_s with pH_∞ for different system parameters. This streaming current when multiplied by the streaming electric field produces the net output power [see Figures 3.10-3.13(c)], which follows the same trend with the different parameters as the electric field E_s. Therefore, we witness an increase in power with weaker c_∞ [see Figure 3.10(c)], for a larger brush height [see Figure 3.11(c)], for a larger pK_a for an acidic pH [see Figure 3.12(c)], for a larger pK_b for a basic solution [see Figure 3.13(c)], for smaller pH_∞ for acidic solution [see Figures 3.10-3.13(a)] (except for very small pH_∞ where the hydrogen ion number density dictates the EDL thickness and this ensures a maximum in the magnitude of power at an intermediate pH_∞), and for larger pH_∞ for basic solution [see Figures 3.10-3.13(a)] (except for very large pH_∞ where the hydroxyl ion number density dictates the EDL thickness and this ensures a minimum or a negative maximum in the magnitude of power at an intermediate pOH_∞). Very

much like E_s, here too we ensure a large P for both large and small pH_∞. Finally, in Figures 3.10-3.13(d), we show the variation in the efficiency ξ in the electrokinetic (or electrochemomechanical) energy conversion. The trend with respect to different parameters is exactly identical to that of the power variation. Most importantly, here too, we ensure a significant conversion efficiency for both large and small pH.

3.4 Discussions

3.4.1 Neglecting the PE brush configurational details

In the development of our theoretical model we have neglected the configurational details of the PE brush. In other words, we have assumed a constant salt-concentration-independent height of the PE brush while developing our model. As we have established in our previous papers [1,85], such an assumption is only valid if the factors dictating the PE brush configuration [namely the elastic (F_{el}) and the excluded volume (F_{EV}) energies] are decoupled from the corresponding electrostatic effects [namely the energy associated with the PE charge (F_{elec}) and that associated with the induced EDL (F_{EDL})]. Such decoupling is possible if either $F_{el}+F_{EV} \gg F_{elec}+F_{EDL}$ (which occurs when $\sigma \gg \sigma_c$) or $F_{el}+F_{EV} \ll F_{elec}+F_{EDL}$ (which occurs when $\sigma \ll \sigma_c$). Here σ is the grafting density and $\sigma_c \approx a^{-1}t^{-1}$ (where a is the Kuhn length and t is the thickness of the polymer brush molecule) is the critical grafting density. Here we assume that either of these conditions ($\sigma \gg \sigma_c$ or $\sigma \ll \sigma_c$) has been satisfied. Of course, in addition to the above conditions, we need additional constraint on the value of σ. For example, we need to ensure that σ is always large enough to ensure that

the grafted polymers may form the brushes, i.e., $\sigma \gg a^{-2}N^{-6/5}$ [1]. Furthermore, σ needs to be small enough to ensure that the grafted brushes on opposing nanochannel walls do not interpenetrate, i.e., $\sigma \ll h^3 a^{-4} N^{-3} t^{-1}$ [1]. Therefore, in summary, our model is valid for $\sigma \ll \sigma_c$ or $\sigma \gg \sigma_c$ and $a^{-2}N^{-6/5} \ll \sigma \ll h^3 a^{-4} N^{-3} t^{-1}$ [1].

It is worthwhile to note here that most of the papers studying the liquid flows in nanochannels grafted with PE brushes have considered such salt-concentration-independent brush height [13,18,19,41,84,92,92,117–123] (or the brush height in the decoupled regime). Our paper [1] unravelled for the first time the physical conditions under which such decoupling is allowed. In another paper [85], we provided examples of experimental studies [124–127] where the above condition of decoupling can be safely employed while describing the PE brush electrostatics. In a recent couple of papers we have considered a simplistic system (a nanochannel grafted with end-charged brushes) and have provided for the first time the calculations for the liquid flows in PE-brush-grafted nanochannels where the brush configuration is obtained through a self-consistent thermodynamic analysis [111,128]. In these papers, we employed the Alexander-de-Gennes model [2–4] to describe the monomer configuration. Such a situation was afforded by the fact that the PE charge was localized at the non-grafted end of the brush. On the other hand, for the present case where we consider a backbone-charged pH-responsive brush, such simplistic modeling will not be possible and any thermodynamically self-consistent approach would necessitate an analysis that remains missing in the literature despite the significant efforts by previous researchers [40]. In one of our papers [16], we pinpoint that this lacuna stems from considering a Boltzmann distribution description of the hydrogen ions

even within the PE brush layer. Therefore, a self-consistent analysis for the present problem would first require a self-consistent thermodynamic analysis of the pH and pOH responsive PZI brushes, which is beyond the scope of the present study.

3.4.2 Choice of the cubic monomer density distribution

Despite considering a decoupled regime, we would still need to know the dimensionless distribution of the PZI chargeable sites φ along the height of the PE brush. In several of our previous papers, we have described the need for considering a *non-unique* cubic distribution of these chargeable sites in order to ensure a continuity in the hydrogen and hydroxyl ion concentration distribution [16, 18, 84, 85]. This continuity would have been achieved by default had we been able to obtain a fully self-consistent thermodynamic description of the pH-responsive PE brushes. No study has been able to achieve that yet. Under these circumstances, the consideration of this cubic monomeric distribution is the best description of φ that one might achieve for a pH-responsive PE brush.

3.5 Conclusions

Here for the first time, we propose a design that uses a PZI-brush-grafted-nanochannel for the electrokinetic energy conversion. The unique ability of the PZI to express significant (but opposite charges) at extreme ends of the pH spectrum has been leveraged in this design to generate electrokinetic power from a pressure-driven transport across a wide range of pH spectrum. Typically, the pH-responsiveness of

nanochannels (with and without the PE brush grafting) enforces a narrow operating pH window for the maximum power generation. Use of PZI brushes expands that window and allows a large power generation across wide ranges (both large and small) pH values.

Chapter 4: Conclusion

We once again review the methods used in this thesis that helped provide us with results of electrokinetics of pH-dependent brushes. We first discuss the necessary decoupling regime that set up our governing equations for electrostatic contributions. Following, we disclose how we solve for the coupled electrostatic potential and ion number distribution using a constant brush height and other system parameters. We next discuss solution of the integro-differential equation between the streaming potential and velocity field. Finally, we discuss the results of energy conversion of polyelectrolyte brushes as well as electrokinetics of polyzwitterionic brushes in nanochannels.

Polyelectrolyte brushes have been proven to be useful for a vast number of applications. Our research focuses on how grafted PE brushes can induce an electric current from the fluid flow in a nanochannel. We were able to do this by simplifying our calculations by assuming a constant brush height. This assumption is only viable when decoupling the electrostatic effects of a PE brush from the excluded volume and entropic effects. When the magnitudes of the excluded volume and entropic contributions are much greater or much smaller than electrostatic effects, this

decoupling regime is possible and we can assume a constant brush height that will not be dynamically affected by the electrostatics of the channel. This sets up our governing equations to be solved for two particular cases of PE brush application. We first examine the effects of nanochannels grafted with PE brushes that exhibit a pH-dependent charge density. After decoupling the excluded volume and entropic effects, we can minimize a new free energy equation consisting of only the electrostatic effects of the brush and the contributions from the electric double layer (EDL) of the channel. Our free energy density function is itself a function of the electrostatic potential of the PE brush and ion number densities. Minimizing this equation gives us the equations for electrostatic potential and ion number densities. These distributions are then used to solve the velocity profile and the induced streaming potential and the electrokinetic energy conversion in presence of an applied pressure gradient. The electrochemomechanical energy conversion in pH-dependent charged polyelectrolytes is one example of a PE brush's application. We observed a 3-5% energy conversion efficiency for this particular method of induced electrokinetic energy generation. We then expand our research by applying this same method of PE brush electrokinetics into nanochannels grafted with polyzwitterionic brushes. Because polyzwitterionic (PZI) brushes display both positive and negative charges, we can now manipulate the system parameters to generate electric charges in both acidic and basic solutions, widening our scope applicability. Nanochannels grafted with polyelectrolyte brushes have been proven to be useful for a great number of applications. We've demonstrated in this thesis that this system is capable of generating electric energy from conversion of chemical and mechanical energy. We also notice that we can expand the use of

these pH-dependent brushes in both acidic and basic solutions. We hope our research can shed light on the usefulness of polyelectrolyte brushes to be further implemented into the sciences and future research.

Bibliography

[1] G. Chen and S. Das, J. Phys. Chem. B **119**, 12714 (2015).

[2] S. Alexander, J. Phys., **38**, 977 (1977).

[3] P.-G. de Gennes, J. Phys., **37**, 1443 (1976).

[4] P.-G. de Gennes, Macromolecules, **13**, 1069 (1980).

[5] R. R. Netz and D. Andelman, Phys. Rep. **380**, 1 (2003).

[6] S. T. Milner, Science **251**, 905 (1991).

[7] S. T. Milner, T. A. Witten and M. E. Cates, Europhys. Lett. **5**, 413 (1988).

[8] S. T. Milner, T. A. Witten and M. E. Cates, Macromolecules **21**, 610 (1988).

[9] A. M. Skvortsov, I. V. Pavlushkov, A. A. Gorbunov, Y. B. Zhulina, O. V. Borisov and V. A. Pryamitsyn, J. Polym. Sci., Part B: Polym. Phys. **30**, 1706 (1988).

[10] Y. B. Zhulina, V. A. Pryamitsyn and O. V. Borisov, Pol. Sci. U.S.S.R. **31**, 205 (1989).

[11] E. B. Zhulina, O. Borisov, V. A. Pryamitsyn and T. M. Birshtein, Macromolecules **24**, 140 (1991).

[12] C. M. Wijmans, J. M. H. M. Scheutjens, and E. B. Zhulina, Macromolecules **25**, 2657 (1992).

[13] S. Chanda, S. Sinha, and S. Das, Soft Matt. **10**, 7558 (2014).

[14] S. Chanda and S. Das, Phys. Rev. E. **89**, 012307 (2014).

[15] S. Das, Collod. Surf. A **462**, 69 (2014).

[16] G. Chen and S. Das, RSC Adv. **5**, 4493 (2015).

[17] K. McDaniel, F. Valcius, J. Andrews, and S. Das, Colloid Surf. B **127**, 143 (2015).

[18] G. Chen and S. Das, J. Appl. Phys. **117**, 185304 (2012).

[19] G. Chen and S. Das, J. Colloid Interface Sci. **445**, 357 (2015).

[20] J. Andrews and S. Das, RSC Adv. **5**, 46873 (2015).

[21] A.F. Morrison and J.F. Osterle, J. Chem. Phys. **43**, 2111 (1965).

[22] J. Yang, F. Lu, L. W. Kostiuk, D. Y. and Kwok, J. Micromech. Microeng. **13**, 963 (2003).

[23] J. F. L. Duval, R. Zimmermann, A.L. Cordeiro, N. Rein, C. Werner, Langmuir **25**, 10691 (2009).

[24] J. F. L. Duval, D. Kütter, C. Werner, and R. Zimmermann, Langmuir **27**, 10739 (2011).

[25] E. Donath and E. Voigt, J. Colloid Interface Sci. **109**, 122 (1986).

[26] H. J. Keh and Y. C. Liu, J. Colloid Interface Sci. **172**, 222 (1995).

[27] H. J. Keh and J. M. Ding, J. Colloid Interface Sci. **263**, 645 (2003).

[28] H. Ohshima and T. Kondo, J. Colloid Interface Sci. **135**, 443 (1990).

[29] M. V. Starov and Y. E. Solomentsev, J. Colloid Interface Sci. **158**, 166 (1993).

[30] M. V. Starov and Y. E. Solomentsev, J. Colloid Interface Sci. **158**, 166 (1993).

[31] H. C. Ma and H. J. Keh, J. Colloid Interface Sci. **313**, 686 (2007).

[32] J. F. L. Duval and H. P. van Leeuwen, Langmuir **209**, 10324 (2004).

[33] S. Das, M. Banik, G. Chen, S. Sinha, R. Mukherjee, Soft Matt. **11**, 8550 (2015).

[34] S. P. Adiga and D. W. Brenner, Macromolecules **40**, 1342 (2007).

[35] S. P. Adiga and D. W. Brenner, J. Funct. Biomater **3**, 239 (2012).

[36] H. Daiguji, P. Yang, A. J. Szeri and A. Majumdar, Nano Lett. **4**, 2315 (2004).

[37] F. H. J. van der Heyden, D. J. Bonthuis, D. Stein, C. Meyer, and C. Dekker, Nano Lett. **7**, 2232 (2006).

[38] O. Azzaroni, J. Pol. Sci **50**, 3225 (2012).

[39] Y. B. Zhulina and O. V. Borisov, J. Chem. Phys. **107**, 5952 (1997).

[40] Y. B. Zhulina and O. V. Borisov, Langmuir **27**, 10615 (2011).

[41] Z. Milne, L. H. Yeh, T. H. Chou, and S. Qian, J. Phys. Chem. C **118**, 19806 (2014).

[42] H. Ohshima, Adv. Colloid Interface Sci. **62**, 189 (1995).

[43] H. Ohshima, Soft Matt. **8**, 3511 (2012).

[44] A. C. Barbati and B. J. Kirby, Soft Matt. **8**, 10598 (2012).

[45] H. Ohshima, Sci. Technol. Adv. Mater. **10**, 063001 (2009).

[46] J. F. L. Duval and F. Gaboriaud, Curr. Opin. Colloid Interface Sci. **15**, 184 (2010).

[47] J. F. L. Duval, J. Merlin and P. Anantha, Phys. Chem. Chem. Phys. **13**, 1037 (2011).

[48] S. Chakraborty and S. Das, Phys. Rev. E **77**, 037303 (2008).

[49] S. Das and S. Chakraborty, Langmuir **25**, 9863 (2009).

[50] T. Das, S. Das, and S. Chakraborty, J. Chem. Phys. **130**, 244904 (2009).

[51] S. Das and S. Chakraborty, Langmuir **26**, 11589 (2010).

[52] K. F. Freed and S. F. Edwards, J. Chem. Phys. **61**, 3626 (1974).

[53] P. G. de Gennes, Macromolecules **9**, 594 (1976).

[54] J. Klein, Colloid. Surf. A **86**, 63 (1994).

[55] A. Bandopadhyay, J. Dhar, and S. Chakraborty, Phys. Rev. E **88**, 033014 (2013).

[56] A. Bandopadhyay and S. Chakraborty, Appl. Phys. Lett. **101**, 153112 (2012).

[57] R. Zimmermann, D. Romeis, I. Bihannic, M. C. Stuart, J-W.

[58] R. Zimmermann, S. S. Dukhin, C. Werner, and J. F. L. Duval, Curr. Opin. Colloid Interface Sci. **18**, 83 (2013).

[59] J. F. L. Duval, D. Kütter, M. Nitschke, C. Werner, and R. Zimmermann, J. Colloid Interface Sci. **362**, 439 (2011).

[60] R. Zimmermann, D. Kuckling, M. Kaufmann, C. Werner, and J. F. L. Duval, Langmuir **26**, 18169 (2010).

[61] S. T. Milner, T. A. Witten, and M. E. Cates, Europhys. Lett. **5**, 413 (1988).

[62] S. T. Milner, T. A. Witten, and M. E. Cates, Macromolecules **21**, 2610 (1988).

[63] S. T. Milner, T. A. Witten, and M. E. Cates, Macromolecules **853**, 22 (1989).

[64] K. N. Witte, S. Kim, and Y.-Y. Won, J. Phys. Chem. B **113**, 11076 (2009).

[65] Q. Wang, T. Taniguchi, and G. H. Fredrickson, J. Phys. Chem. B **108**, 6733 (2004).

[66] G. Quan, M. Wang, and C. Tong, Polymer **55**, 6604 (2014).

[67] M. Wang and C. Tong, RSC Adv. **4**, 20769 (2014).

[68] A. K. Dolan and S. F. Edwards, Proc. R. Soc. London Ser. A **337**, 509 (1974).

[69] A. K. Dolan and S. F. Edwards, Proc. R. Soc. London Ser. A **427**, 343 (1975).

[70] R. Israels, F. A. M. Leermakers, G. J. Fleer, and E. B. Zhulina, Macromolecules **27**, 3249 (1994).

[71] Y. V. Lyatskaya, F. A. M. Leermakers, G. J. Fleer, E. B. Zhulina, and T. M. Birshteint, Macromolecules **28**, 3562 (1995).

[72] K. Knop, R. Hoogenboom, D. Fischer, and U. S. Schubert, Angew. Chem. Int. Ed. **49**, 6288 (2010).

[73] J. S. Suk, Q. Xu, N. Kim, J. Hanes, and L. M. Ensign, Adv. Drug Deliver. Rev. *doi* : 10.1016/*j.addr*.2015.09.012 (2015).

[74] H. ShamsiJazeyi, C. A. Miller, M. S. Wong, J. M. Tour, and R. Verduzco, J. Appl. Polym. Sci. **131**, 40576 (2014).

[75] G. W. de Groot, M. G. Santonicola, K. Sugihara, T. Zambelli, E. Reimhult, J. Vörös, and G. J. Vancso, ACS Appl. Mater. Interface. **5**, 1400 (2013).

[76] B. Yameen, M. Ali, R. Neumann, W. Ensinger, W. Knoll, and O. Azzaroni, J. Am. Chem. Soc. **131**, 2070 (2009).

[77] M. Ali, B. Yameen, R. Neumann, W. Ensinger, W. Knoll, and O. Azzaroni, J. Am. Chem. Soc. **130**, 16351 (2008).

[78] M. Ali, B. Schiedt, R. Neumann, and W. Ensinger, Macromol. Biosci. **10**, 28 (2010).

[79] S. Umehara, M. Karhanek, R. W. Davis, and Nader Pourmand, Proc. Natl. Acad. Sci. **106**, 4611 (2009).

[80] M. Ali, B. Yameen, J. Cervera, P. Ramirez, R. Neumann, W. Ensinger, W. Knoll, and O. Azzaroni, J. Am. Chem. Soc. **132**, 8338 (2010).

[81] B. Vilozny, A. L. Wollenberg, P. Actis, D. Hwang, B. Singaram, and N. Pourmand, Nanoscale **5**, 9214 (2013).

[82] M. Ali, P. Ramirez, S. Mafe, R. Neumann, and W. Ensinger, ACS Nano **3**, 603 (2009).

[83] S. Moya, O. Azzaroni, T. Farhan, V. L. Osborne, and W. T. S. Huck, Angewandte Chem. **44**, 4578 (2005).

[84] J. Patwary, G. Chen, and S. Das, Microfluid. Nanofluid. **20**, 37 (2016).

[85] H. Li, G. Chen, and S. Das, Colloid Surf. B **147**, 180 (2016).

[86] G. Chen and S. Das, Electrophoresis **38**, 720 (2017).

[87] B. Yameen, M. Ali, R. Neumann, W. Ensinger, W. Knoll and O. Azzaroni, Nano Lett. **9**, 2788 (2009).

[88] M. Tagliazucchi, O. Azzaroni, and I. Szleifer, J. Am. Chem. Soc. **132**, 12404 (2010).

[89] J-Y. Lin, C-Y. Lin, J-P. Hsu, and S. Tseng, Anal. Chem. **88**, 1176 (2016).

[90] Y. Ma, L-H. Yeh, C-Y. Lin, L. Mei, and S. Qian, Anal. Chem. **87**, 4508 (2015).

[91] S. Xue, L. H. Yeh, Y. Ma, and S. Qian, J. Phys. Chem. C **118**, 6090 (2014).

[92] C. Zhou, L. Mei, Y-S. Su, L-H.Yeh, X. Zhang, and S. Qian, Sens. Actuat. B **229**, 305 (2016).

[93] M. Ali, B. Schiedt, K. Healy, R. Neumann, and W. Ensinger, Nanotechnology **19**, 085713 (2008).

[94] F. M. Gilles, M. Tagliazucchi, O. Azzaroni, and I. Szleifer, J. Phys. Chem. C **120**, 4789 (2016).

[95] M. Tagliazucchi and I. Szleifer, Soft Matt. **8**, 7292 (2012).

[96] A. B. Lowe, C. L. McCormick, Polyelectrolytes and Polyzwitterions: Synthesis, Properties, and Applications, ACS Symposium Series, American Chemical Society (2006).

[97] M. Ilcikova, J. Tkac, and P. Kasak, Polymers **7**, 2344 (2015).

[98] E. E. Urena-Benavides, E. L. Lin, E. L. Foster, Z. Xue, M. R. Ortiz, Y. Fei, E. S. Larsen, A. A. Kmetz, B. A. Lyon, E. Moaseri, C. W. Bielawski, K. D. Pennell, C. J. Ellison, and K, P. Johnston, Ind. Eng. Chem. Res. **55**, 1522 (2016).

[99] T. A. Saleh, I. B. Rachman, and S. A. Ali, Sci. Rep. **7**, 4573 (2017).

[100] W. Xiao, J. Lin, M. Li, Y. Ma, Y. Chen, C. Zhang, D. Li, and H. Gu, Contrast Media Mol. Imaging **7**, 320 (2012).

[101] Y. Zhao, Y. Chen, X. Xiong, X. Sun, Q. Zhang, Y. Gan, L. Zhang, and W. Zhang, J. Chromatogr. A **1482**, 23 (2017).

[102] C. Monteil, N. Bar, A. Bee, and D. Villemin, Beilstein J. Nanotechnol. **7**, 1447 (2016).

[103] L. C. Fidale, M. Nikolajski, T. Rudolph, S. Dutz, F. H. Schacher, and T. Heinze, J. Colloid Interface Sci. **390**, 25 (2013).

[104] M. Chen, W. H. Briscoe, S. P. Armes, and J. Klein, Science **323**, 1698 (2009).

[105] M. Chen, W. H. Briscoe, S. P. Armes, H. Cohen, and J. Klein, Eur. Pol. J. **47**, 511 (2011).

[106] O. Azzaroni, A. A. Brown, and W. T. S. Huck, Angewandte Chem. **118**, 1802 (2006).

[107] N. Cheng, A. A. Brown, O. Azzaroni and W. T. S. Huck, Macromolecules **41**, 6317 (2008).

[108] M. Kobayashi and A. Takahara, Pol. Chem. **4**, 4987 (2013).

[109] Y. Higaki, M. Kobayashi, D. Murakami, and A. Takahara, Pol. J. **48**, 325 (2016).

[110] Z. Zeng, L. H. Yeh, M. Zhang, and S. Qian, Nanoscale **7**, 17020 (2015).

[111] G. Chen, H. S. Sachar, and S. Das, Soft Matt. $DOI : 10.1039/C8SM00768C$ (2018).

[112] T. Nguyen, Y. Xie, L. J. de Vreede, A. van den Berg, and J. C. T. Eijkel, Lab Chip, **13**, 3210 (2013).

[113] F. H. J. van der Heyden, D. J. Bonthuis, D. Stein, C. Meyer, and C. Dekker, Nano Lett. **7**, 1022 (2007).

[114] S. Baldessari and J. G. Santiago, J. Colloid Interface Sci. **325**, 526 (2008).

[115] S. Das, A. Guha, and S. K. Mitra, Anal. Chim. Acta **804**, 159 (2013).

[116] S. Das, S. Chanda, J. C. T. Eijkel, N. R. Tas, S. Chakraborty, and S. K. Mitra, Phys. Rev. E **90**, 043011 (2014).

[117] A. Poddar, D. Maity, A. Bandopadhyay, and S. Chakraborty, Soft Matt. **12**, 5968 (2016).

[118] L-H. Yeh, M. Zhang, N. Hu, S. W. Joo, S. Qian, and J-P. Hsu, Nanoscale **4**, 5169 (2012).

[119] L-H. Yeh, M. Zhang, N. Hu, S. W. Joo, S. Qian, and J-P. Hsu, Anal. Chem. **84**, 9615 (2012).

[120] L. Benson, L-H. Yeh, T-H. Chou, and S. Qian, Soft Matter **9**, 9767 (2013).

[121] F. Li, Y. Jian, L. Chang, G. Zhao, and L. Yang, Colloid. Surf. B **147**, 234 (2016).

[122] Q. Cao and H. You, Polymers **8**, 438 (2016).

[123] F. Li, Y. Jian, Z. Xie, Y. Liu, and Q. Liu, RSC Adv. **7**, 782 (2017).

[124] M. Hoffmann, A. Jusufi, C. Schneider, and M. Ballauff, J. Colloid Interface Sci. **338**, 566 (2009).

[125] X. Guo and M. Ballauff, Langmuir **16**, 8719 (2000).

[126] X. Wang, J. Xu, L. Li, S. Wu, Q. Chen, Y. Lu, M. Ballauff, and X. Guo, Macromol. Rapid Commun. **31**, 1272 (2010).

[127] X. Guo and M. Ballauff, Phys. Rev. E **64**, 051406 (2001).

[128] G. Chen and S. Das, J. Phys. Chem. B **121**, 3130 (2017).